Journal of Sustainable Food, Water, Energy and Environment (JSFWEE)

Publisher

Faculty of Graduate Studies and Environmental Research, Sohag University, Egypt

University president

Prof. Dr. Hassan Noaman

Editor-in-Chief

Prof. Dr. Sodky Hamed Mohamed

Managing Editor

Dr. Hamdy Abdelhamed Mohamed

Executive Editor

Dr. Amira Maher Ahmed

Volume 1. April 2025

Print ISSN 3062-5513   **Online ISSN 3062-5521**

Journal of Sustainable Food, Water, Energy and Environment (JSFWEE)

(Faculty of Graduate Studies and Environmental Research, Sohag University)

The JSFWEE is a peer-reviewed specialized journal. It is published both online and in print. The journal published biannually by Faculty of Graduate Studies and Environmental Research at Sohag University which is concerned with publishing original, methodological, and plagiarism-free papers in theoretical and experimental papers of all sustainable issues of food, water, energy and environment as well as the intersection of these two fields with each other and with other fields of research. Its editorial board includes efficient and reputable professors. In addition, the manuscripts are reviewed by experienced, reputable reviewers. The JSFWEE is an opportunity for international researchers to publish original papers and materials publishes original research articles, comprehensive review articles, short communications and notes in English

Aims and scope of the journal

The Journal of sustainable food, water energy and environment (JSFWEE) is a multidisciplinary peer-reviewed international journal. JSFWEE aims to improve and disseminate knowledge on the methods, technologies and policies needed to develop and sustain food, water, energy and the environment by decoupling growth from natural resources and replacing it with a knowledge-based economy, taking into account its economic, environmental and social pillars, as well as methods for assessing and measuring the sustainability of development, in relation to food, water, energy and environment production systems and their many combinations. JSFWEE publishes theoretical and experimental papers of basic and applied research. The scope of JSFWEE includes all sustainable issues of food, water, energy and environment with a wide but in-depth coverage. JSFWEE publishes original research articles, comprehensive review articles, short communications and notes to the editor within the scope of the journal.

Objectives of the journal

1. To publish innovative and original research that fulfill the methodologies and standards of the fields of food, water, energy and environment sustainability.
2. To disseminate knowledge on the methods, technologies and policies needed to develop and sustain food, water, energy and the environment by decoupling growth from natural resources and replacing.
3. Providing a publishing platform for researchers that links food, water, energy and environment sustainability.

4. To feature current theories, concepts, ideas and trends in the fields of food, water energy and environment sustainability.

Publication Frequency

The JSFWEE is published biannually in March and September.

Fields of specialization

The scope of the journal includes the following specific areas:

- **All disciplines of food sustainability, Agricultural and food economics**
- **Urban agriculture**
- **Climate-smart food systems**
- **Crop biology and sustainability**
- **Agroecology and ecosystem services**
- **Nutrition and sustainable diets agro-food safety**
- **Social movements, institutions, and governance**
- **Sustainable food processing**
- **Water-smart food production.**
- **All disciplines of water sustainability**
- **Waste management in agroecosystems**
- **Ecological and human risk assessment**
- **Environmental system modelling and optimization**
- **Biodiversity conservation and ecosystems**
- **Social, economic and policy aspects of environmental management**
- **Targets, Technologies and strategies for developing the decision-making framework in the water sector**
- **Urban planning addressing water and environmental sustainability**
- **Hydrology and hydrogeology**
- **Atmospheric pollutants and trace gases, solid and hazardous waste management**
- **Probabilistic modelling of water resources**
- **Related researched on Environmental Sciences**
- **Uncertainty assessment in impact studies**
- **Energy and nutrient recovery in wastewater treatment**
- **All disciplines of energy sustainability, Renewable Energy Sources**
- **Economics of sustainable energy systems**
- **Educational and technological research papers on sustainable Energy**
- **Sustainable energy efficiency and sustainable energy conservation**
- **Photovoltaics**
- **Combined and hybrid sustainable energy systems**
- **Smart grids**
- **Carbon capture and storage**
- **Sustainability in the urban environment**
- **Energy and environmental policies**
- **Social dimensions of energy and sustainability.**
- **Concentrated Solar Technology**
- **Biomass and bioenergy**
- **Marine and hydropower energy systems**
- **Environmental chemistry and biology**

Editorial board

Contents

Volume 1. April 2025

Journal of sustainable food, water, energy and environment

Highly sensitive TiO_2 based photodetector for environmental sensing applications

S.H. Mohamed[1,2], Mohamed Rabia[3], M. A. Awad[2], Mohamed Asran Hassan[2]

[1]Falculty of Graduate Studies and Environmental Research, Sohag University, 82524 Sohag, Egypt

[2]Physics Department, Faculty of Science, Sohag University, 82524 Sohag, Egypt

[3]Nanomaterials Science Research Laboratory, Chemistry Department, Faculty of Science, Beni-Suef University, Beni-Suef, 62514, Egypt.

Received: 2 Jan. 2025, Revised: 17 Jan. 2025, Accepted: 31 Jan. 2025 Published online: 1 Apr. 2025

Abstract: TiO_2 thin films were fabricated using reactive direct current magnetron sputtering for the possible utilization as visible and/or IR-light photodetectors. The structure, chemical composition, morphology, optical and I-V characteristics were examined. X-ray diffraction inferred the existence of body centered tetragonal anatase crystallographic phase oriented around (101) plain. The chemical compositional analysis via EDAX indicated $TiO_{2.1}$ stoichiometry. Nanoparticle morphology that is uniformly distributed were observed by SEM investigations. High transmittance over the visible and near spectral ranges with optical band gap of 3.29 eV were observed for the TiO_2 thin films. The generated light current values at 1 V bias voltage were 0.251, 0.160 and 0.149 µA/cm^2 for illumination with light of 440, 540 and 730 nm, respectively. The reported TiO_2 based photodetector has good sensitivity comparable with the previously published works which infers that it may be used in environmental sensing applications.

Keywords: TiO_2 thin films; structural propertis ;morphology; optical characteristics; photodetector

1. Introduction

Now a days monitoring the environment requires a broad-range of photodetectors from the ultraviolet (UV) to the infrared (IR) [1,2]. For example, detection of pollution mainly depends on UV spectroscopy, where the detectors measure the absorption lines strength for these pollutants such as ozone, nitrous oxides, and sulfur dioxide. Fluorescence spectroscopy capable of detecting very small amounts of pollutants such as sulfur oxides, benzene, xylene and toluene, which can be measured at a parts-per-billion level [3]. To monitor solid particulates in water and air, more straightforward techniques are utilized. In this case, the quantity of scattered light via the particles gives a measure for levels of pollution. In many cases ample light is available, so photodetectors may be utilized, taking advantage of their fast response times and robustness [4].

As a semiconductor titanium dioxide (TiO_2) is characterized by a wide band gap (> 3.0 eV), low cost, high stability and photo-active properties. Therefore, it has received a significant interest and it has found numerous applications in various fields such as solar cells [5], energy storage [6], photocatalytic, antioxidant and antibacterial applications [7,8], photodetectors [9], etc.

In the field of photodetectors TiO_2 based photodetectors have common view over photodetectors including better control, good sensing properties, enhanced catalytic activity, self-sufficiency, better communication proficiencies, response speed and high sensitivity with low cost user-friendly [10]. Therefore, TiO_2 based photodetectors have become an important semiconductor device because of their applicability in different day-to-day life appliances like environmental monitoring, compact smoke detectors, optical communication, imaging, remote control, chemical analysis and disk players [10-14]. However, there is remaining a challenging task which is the fabrication of a very thin TiO_2 based photodetector device [15]. Therefore, in this work the TiO_2 thin films with thickness of 230 nm were prepared using direct current (dc) reactive magnetron sputtering as visible and/or IR-light photodetectors. Moreover, the crystal structure, morphology and optical characteristic of the films were investigated.

2. Experimental

TiO_2 thin films were deposited using dc reactive magnetron sputtering from metallic Ti target. The preparation was achieved on FTO, glass and Si (100) substrates which were previously heated to 200°C.

* Corresponding author E-mail: abo_95@yahoo.com
Print ISSN 3062-5513 Online ISSN 3062-5521

Deposition was started after reaching a base pressure of 3.1 × 10^{-7} mbar. Ar and O_2 of 75 and 25 sccm, respectively, were used for the deposition of the films. The deposition was achieved at constant power of 100 W. The working pressure was 1.2 × 10^{-2} mbar. The film thickness was fixed to 230 nm by controlling the deposition time.

ZEISS scanning electron microscope (SEM) was used to examine the surface morphology. The chemical composition of the films was estimated from the energy dispersive analysis of X-ray (EDAX) unit which is attached to the SEM. The crystallographic identification was achieved using X-ray diffraction (XRD) model Bruker D8 ADVANCE diffractometer. The PEAK UV-Vis-NIR spectrophotometer (model C-7200) was utilized to measure transmittance (T) and the reflectance (R) of the films.

The characteristics of the TiO_2 photodetector on FTO substrates were conducted on CHI660E electrochemical workstation. The I-V measurements were carried out in the voltage range from -1 to +1 V. 100 mW/cm^2 xenon lamp was utilized as simulated light source, in which glass/FTO/TiO_2 presents the photoelectrode. Silver paste was used to make the electrodes on two sides of the photodetector. The effect of monochromatic light wavelength on the performance the deposited photodetector was investigated with 440, 540 and 730 nm wavelengths. The light reproducibility was assessed via on/off chopped current measurements with time. The measurements were done at atmospheric conditions and at room temperature.

3. Results and discussions

3.1 EDAX, XRD, SEM and optical examinations

Fig. 1 shows EDAX spectrum of sputtered film on Si (100) substrate. Oxygen and titanium peaks are existing together with silicon and small carbon peaks. The silicon peak comes from the Si (100) substrate and the carbon peak comes from the contamination of the film's surface by the hydrocarbons after sputtering or during the EDAX measurement. The estimated Ti and O atomic percentage ratios are 31.76 at.% and 68.24 at.%, respectively. Thus, the obtained stoichiometry is $TiO_{2.1}$. The excess oxygen in the film may be physically trapped, chemically bonded and/or adsorbed on the surface [16].

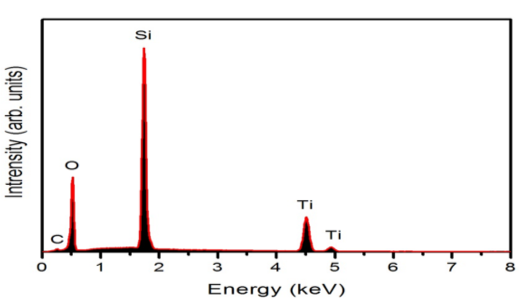

Fig. 1: Typical EDAX spectra of TiO_2 thin film deposited on Si (100) substrate.

Fig. 2 displays the XRD pattern of the sputtered TiO_2 thin film on glass substrate. The pattern of pure TiO_2 displays several crystalline peaks which are indexed to body centered tetragonal anatase crystallographic phase (COD: 01-089-4921). The phase is highly oriented around (101) plain. The crystallite size (L) is calculated from the Scherrer equation using (101) peak.

$$L = \frac{K\lambda}{\beta cos\theta} \quad (1)$$

where λ (nm) is the wavelength of the XRD radiation, β is the full width at half maximum of peaks (101) in radian located and K is the shape factor which is usually taken as about 1. The obtained L value is found to be 18.3 nm.

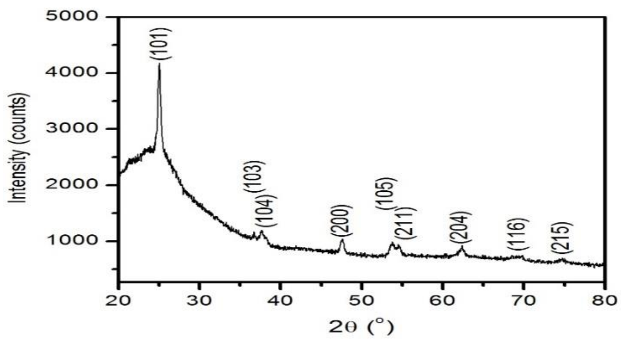

Fig. 2: XRD pattern of TiO_2 thin film deposited on glass substrate.

Fig. 3 presents the surface morphology of the TiO_2 film displayed from SEM. The film exhibits quite homogeneous and uniform nanoparticles morphology. The diameters of nanoparticles are in the range 10–36 nm. Besides to nanoparticles there are small pinholes-like nanodefects. Similar morphology was reported previously for titanium oxynitride films prepared by dc reactive magnetron sputtering [18].

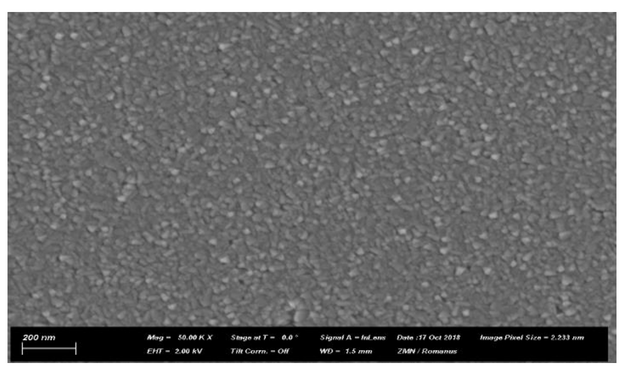

Fig. 3: SEM image of TiO_2 thin film deposited on Si (100) substrate.

The optical reflectance and transmittance of TiO_2 film on glass substrate as functions of wavelength are presented in Fig. 4. The transmittance of TiO_2 is high over the entire visible and near infrared ranges. Some interference fringes are observed in both transmittance and reflectance due to the difference in refractive index between TiO_2 and air, and TiO_2 and glass. The existence of the interference fringes infers the good quality of the films.

The absorption coefficient (α) of TiO_2 film is calculated from the reflectance and transmittance spectra and thickness (d) of the film via the equation:

$$\alpha = \frac{1}{d} ln\left(\frac{1-R}{T}\right) \qquad (2)$$

The optical band gap (Eg) is obtained by proposing allowed indirect transition from Tauc's formula:

$$(\alpha h\nu)^{\frac{1}{2}} = A(h\nu - E_g) \qquad (3)$$

where ν is to the frequency of the incident light and A is a constant. Fig. 4b presents the $(\alpha h\nu)^{\frac{1}{2}}$ versus hν plot with the linear fit to a straight line. The Eg value is obtained through the extrapolation of the linear part to intercept with hν axis. The obtained Eg value is 3.29 eV which is very near to the value 3.2 of bulk anatase [19]. However, it is lower than the values 3.32-374 eV of TiO_2 prepared by reactive dc magnetron sputtering at various working pressures [20].

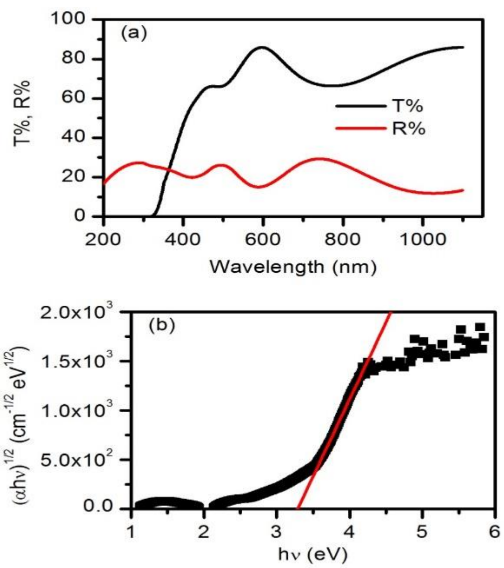

Fig. 4: Optical reflectance and transmittance as a function of wavelength (a), and $(\alpha h\nu)^{\frac{1}{2}}$ versus hν plot (b) for TiO_2 thin film deposited on glass substrate.

3.2 The Photodetector Electrochemical characterization

The response of the deposited FTO/TiO_2 photodetector at different wavelengths of 440, 540 and 730 nm is presented in Fig. 5. Both the dark current (I_{Dr}) and light current (I_{Ph}) increase with bias potential. This is agreement with the reported results for TiO_2 photoelectrodes [21]. It is observed that the generated dark current density (Io) at +1 V has a very low value of 0.046 µA/cm^2, concerned to the original charges of FTO/TiO_2 semiconductor. The generated I_{ph} values at 1 V bias voltage are 0.251, 0.160 and 0.149 µA/cm^2 for illuminated light with 440, 540 and 730 nm, respectively. It is observed that the photodetector responded strongly to the different light wavelengths. During light irradiation electron and hole pairs are photo-produced. Thus, the decrease in I_{Ph} values with increasing wavelength is attributed to the disparity in the capability of the incident photons to generate charge carriers. This infers that the photodetector is capable to respond to various light regions with various sensitivities. The FTO/TiO_2 photodetector has the highest sensitivity in the visible region.

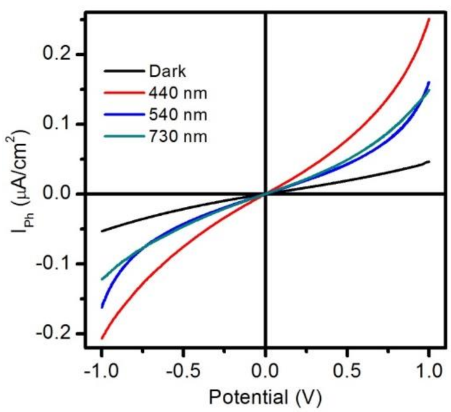

Fig. 5: The response of the deposited FTO/TiO_2 photodetector at different wavelengths.

Fig. 6 displays multiple photo-switching cycles at a bias potential of 1 V. It is observed that the elevation time is almost the same as the decay time. This infers that photogenerated carriers in FTO/TiO_2 photodetector are fast in both generatio n and recombination which confirms the fast charge transport rate. The response speed is a substantial property for the photodetector, which indicates how fast the high- and low-current states can be changed. The response times (fall and rise times) are set as times needed for the current to increase from 10% to 90% or decrease from 90% to 10% of the highest value after on/off cycling. The time of response is almost 6 s. Table 1 shows a comparison between the sum of the devices previously published and the TiO_2 based photodetector reported in this work. The FTO/TiO_2, presented in this work, exhibits higher sensitivity (I_{Ph}/I_{Dr}) compared with other photodetectors.

Material	λ (nm)	Bias (V)	I_{Ph}/I_{Dr}	Ref.
Pt/TiO_2/P-Si (111)/In	405	5	2.32	[22]
TiO_2/water solid-liquid	365	0	200	[23]
Al/CuO/Al	808	5	4.05	[24]
FTO/TiO_2/TNA/water solid–liquid	365	0	200	[25]
Cu/CuO/Ag	UV source	0.01	~69	[26]
In_2O_3/CuO	589	5	2.6	[27]
CuO	250-900	20	1.25-1.8	[28]
FTO/TiO_2	440	1	5.39	This work

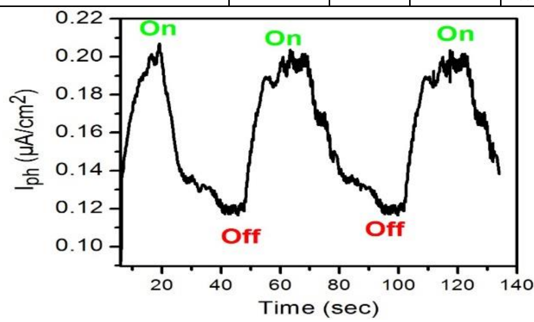

Fig. 6: displays multiple photo-switching cycles at a bias potential of 1 V for FTO/TiO_2 photodetector.

Table 1: Comparison between the present FTO/TiO_2 photodetectors and some of the photodetectors published previously.

4. Conclusion

TiO_2 thin films were deposited on onto glass, Si (100) and FTO substrates. XRD, SEM and EDAX analysis revealed single body centered tetragonal anatase crystallographic with nanoparticle morphology and $TiO_{2.1}$ stoichiometry that contained excess oxygen. The films have high transmittance over the visible and near infrared spectral ranges. The E_g value was 3.29 eV. The I_{ph} values at 1 V bias voltage were 0.251, 0.160 and 0.149 μA/cm^2 when irradiated with light of 440, 540 and 730 nm wavelength, respectively. The FTO/TiO_2 photodetector has good sensitivity and it may be used in environmental sensing applications.

Conflicts of interests

The authors declare that that present work does not have conflict of interest.

Author Contribution

Material preparation, data collection and analysis were performed by S.H. Mohamed, Mohamed Rabia, M. A. Awad and Mohamed Asran Hassan. The first draft of the manuscript was written by S.H. Mohamed and all authors commented on previous versions of the manuscript. All authors read and approved the final manuscript.

Research Data Policy and Data Availability Statements

The data are available on reasonable request from the corresponding author.

5. References

[1] N. Jain, D. Kumar, K. Bhardwaj, R. K. Sharma, J. Holovsky, M. Mishra, Y. K. Mishra and S. K. Sharma, “Heterostructured core-shell metal oxide-based nanobrushes for ultrafast UV photodetectors”, Mater. Sci. Eng. R, vol. 160, pp. 100826, 2024.

[2] A. B. U. Rahman, S. Begum, N. M. S. Kaawash, M. Y.H. Thabit, D. I. Halge, P. M. Khanzode, S. J. Shaikh, V. N. Narwade, P. S. Alegaonkar and K. A. Bogle, “p-NiO/n-ZnO heterojunctions for visible-blind UV and IR photodetectors: A low-temperature fabrication approach”, Physica B: Cond. Matter., vol. 694, pp. 416478, 2024.

[3] M. Ródenas, T. Vera, A. Muñoz and F. Villanueva, “Advantages and limitations of the analytical methods currently employed for the assessment of inorganic pollutants in indoor and outdoor air”, TrAC- Trends Anal. Chem., vol. 181, pp. 118034, 2024.

[4] Y. Yuan, H. Tao, H. Wang, J. Liu, Y. Zhang, Q. Fu, H. Zhao, T. Di, H. Long and S. Yao, “The effect of UVO treatment on TiO2-MAPbI3 heterostructure photodetector prepared in air atmosphere”, Mater. Sci. Semicond. Process., vol. 172, pp. 108079, 2024.

[5] S. Mathur, V. Bishop, A. Swindle and W. Wei, “Enhanced performance of Bi2S3/TiO2 heterostructure composite films for solar cell applications”, J. Photochem. Photobiol., vol. 25, pp. 100256, 2025.

[6] M. Z. Ullah Shah, J. Feng, F. BiBi, M. Sajjad, M. T. Qureshi, A. Shah, M S. Shah, A. M. Khaled and M. S. Salem, “Enhanced energy storage with TiO2/NiO/ZnO core-shell heterostructures in hybrid battery-supercapacitor applications”, J. Alloys Compod., vol. 1013, pp. 178548, 2025.

[7] N. Thakur, N. Thakur, A. Kumar, V.K. Thakur, S. Kalia, V. Arya, A. Kumar, S. Kumar and G. Z. Kyzas, “A critical review on the recent trends of photocatalytic, antibacterial, antioxidant and nanohybrid applications of anatase and rutile TiO2 nanoparticles”, Sci. Total Environ., vol. 914, pp. 169815, 2024.

[8] S. Hassaballa, A Aljabri, S. H. Mohamed, N. M. A. Hadia and M. A. Awad, “Synthesis, structural, photocatalytic, wettability and optical properties of TiO2 films on polymethyl methacrylate substrates”, Phys. Scr.,

vol. 98, pp. 055801, 2023.

[9] S. Izmirli and S. Cavdar, “Effect of film thickness on photodiode and photodetector performance of Titanium dioxide (TiO2) prepared via solution Assisted spin coating method”, Appl. Surf. Sci., vol. 688, pp. 162187, 2025.

[10] C. Ghosh, A. Dey, I. Biswas, R. K. Gupta, V. S. Yadav, A. Yadav, N. Yadav, H. Zheng, M. Henini and A. Mondal, “CuO–TiO2 based self-powered broad band photodetector”, Nano Mater. Sci., vol 6, pp. 345-354, 2024.

[11] M. Zhou, S. Zhang and Y. Wang, “ZnS-shelled and Zn-doped CuInS2 quantum dots for TiO2-based UV photodetectors”, Chem. Phys. Lett., vol. 862, pp. 141861, 2025.

[12] S. Lee, M. Kim, B. J. Ahn and Y. Jang, “Odorant-responsive biological receptors and electronic noses for volatile organic compounds with aldehyde for human health and diseases: a perspective review”, J. Hazard. Mater., vol. 455, pp.131555, 2023.

[13] Y. Shehu, S. A. M. Samsuri, Naser M. Ahmed, S. Aslam, “Fabrication of TiO2 nanoparticles/porous-silicon heterostructure photodetector for UV detection”, Optik, vol 304, pp. 171784, 2024.

[14] J. Chen, J. Xu, L. Kong, S. Shi, J. Xu, S. Gao, X. Zhang and L. Li, “Self-powered SnSx/TiO2 photodetectors (PDs) with dual-band binary response and the applications in imaging and light-encrypted logic gates”, J. Colloid Interface Sci. vol. 663, pp. 336-344, 2024.

[15] Y. Wang, A. J. Muhowski, L. Nordin, S. Dev, M. Allen, J. Allen and D. Wasserman, “High-speed long-wave infrared ultra-thin photodetectors”, APL Photonics vol. 9, pp.016117, 2024.

[16] S.H. Mohamed, O. Kappertza, J.M. Ngaruiya, T.P. Leervad Pedersen, R. Drese and M. Wuttig, “Correlation between structure, stress and optical properties in direct current sputtered molybdenum oxide films”, Thin Solid Films, vol. 429, pp. 135-143, 2023.

[17] B. D. Cullity, “Elements of X-Ray Difraction”, 2nd ed. AddisonWesley, Reading, MA, pp.102, 1979.

[18] A. M. Abd El-Rahman and S. H. Mohamed, “Preparation and characterization of nanostructured titanium oxynitride films for the application in self-cleaning and photoelectrochemical water splitting”, Thin Solid Films, vol. 698, pp. 137864, 2020.

[19] L. Chiodo, J.M. Garcia-Lastra, A. Iacomino, S. Ossicini, J. Zhao, H. Petek and A. Rubio, “Self-energy and excitonic effects in the electronic and optical properties of TiO2 crystalline phases”, Phys. Rev. B: Condens. Matter., vol. 82, pp. 045207, 2010.

[20] F. A. Hernández-Rodríguez, R. Garza-Hernández, M. R. Alfaro-Cruz and L. M. Torres-Martínez, “Tunable structure of TiO2 deposited by DC magnetron sputtering to adsorb Cr (VI) and Fe (III) from water”, Heliyon vol. 10, pp. e27359, 2024.

[21] Z. Li, Z. Li, C. Zuo and X. Fang, “Application of Nanostructured TiO2 in UV Photodetectors: A Review”, Adv. Mater., vol. 34, pp. 2109083, 2022.

[22] A. M. Selman, Z. Hassan, M. Husham and N. M. Ahmed, “A high-sensitivity, fast-response, rapid-recovery p–n heterojunction photodiode based on rutile TiO2 nanorod array on p-Si (111)”, Appl. Surf. Sci., vol. 305, pp. 445-452, 2014.

[23] W.J. Lee and M. H. Hon, “An ultraviolet photo-detector based on TiO2/water solid-liquid heterojunction”, Appl. Phys. Lett. 99 (2011) 251102.

[24] K.M. Chahrour, N.M. Ahmed, M. Hashim, N.G. Elfadill, M. Bououdina, “Self-assembly of aligned CuO nanorod arrays using nanoporous anodic alumina template by electrodeposition on Si substrate for IR photodetectors”, Sens. Actuat. A: Phys., Vol. 239, pp. 209-219, 2016.

[25] Y. Xie, L. Wei, G. Wei, Q. Li, D. Wang, Y. Chen, S. Yan, G. Liu, L. Mei and J. Jiao, “A self-powered UV photodetector based on TiO2 nanorod arrays”, Nanoscale Res. Lett., vol. 8, pp. 188, 2013.

[26] A.M. Anand, A. Raj, J.A. Salam, R.A. Nath and R. Jayakrishnan, “Photoconductivity in self-assembled CuO thin films”, Mater. Renew. Sustain. Energy, vol. 13, pp. 45-58, 2024.

[27] A. M. Abd El-Rahman, S. H. Mohamed, A. Ibrahim, A. A. Alhazime, M. A. Awad, “Optoelectronic characteristics of In2O3/CuO thin films for enhanced vis-light photodetector”, J. Mater. Sci.: Mater. Electron., vol. 35, pp. 1910, 2024.

[28] A. Tripathi, T. Dixit, J. Agrawal and V. Singh, “Bandgap engineering in CuO nanostructures: Dual-band, broadband, and UV-C photodetectors”, Appl. Phys. Lett., vol. 116, pp. 111102, 2020.

Journal of sustainable food, water, energy and environment

Integration of Google Earth Engine and GIS for monitoring and mapping the spatio-temporal of major air pollutants in Sohag Governorate

Abdel-rahman Abdel-wahed Mustafa

Soil and Water Department, Faculty of Agriculture, Sohag University, Sohag, Egypt

Received: 5 Jan. 2025, Revised: 19 Jan. 2025, Accepted: 2 Feb. 2025 Published online: 1 Apr. 2025

Abstract: The present investigation aims to monitor and mapping the spatiotemporal air quality over Sohag Governorate, Egypt. To do so, remote sensing data sets products from the google earth engine (GEE) were integrated with GIS for mapping the major air pollutants. The annually satellite image data of Sentinel-5P for four major pollutants viz., sulfur dioxide (SO_2), nitrogen dioxide (NO_2), ozone (O_3) and carbon mono (CO) for six years from 2019 to 2024. In the studied period, the CO concentrations varied from 28 to 32 ppm whereas, for O_3, NO_2 and SO_2 ranged from 195 to 209, 101 to 140 and 52 to 490 ppb, respectively. The obtained results suggested that the area under study is suffer from low air quality, which affected both environment and the public health.

Keywords: GEE; GIS; air pollutants; remote sensi

1. Introduction

The major environmental problems facing many cities are air pollution due to increased population, traffic, industry, and agricultural biomass burning events, and natural sources of particulate matter, such as dust and sand events and anthropogenic fuel consumption in transportation and industrial activities [1]. Additionally, high concentrations of many air pollutants can cause serious health problems such as pulmonary and cardiovascular diseases [2]. Egypt is one of the developing countries that face challenges in terms of air pollution [1,3-5]. The most common air pollutants include, but not limited to particulate matter (PM2.5, PM10), sulfur dioxide (SO_2), nitrogen dioxide (NO_2), ozone (O_3), methan (CH_4), formaldhyde (CH_2O) and carbon mono and dioxide (CO, CO_2) [6].

Recently, there has been growing interest in the use of satellite-based remote sensing has emerged as a powerful tool for air quality assessment and monitoring. Remote sensing techniques allow for the collection of data on air pollution over both spatial and temporal patterns, which can provide a more comprehensive understanding of air quality than traditional monitoring methods [7]. This approach has been used in several studies to monitor air pollution in urban areas around the world, including Cairo [1]. The tropospheric monitoring instrument (Sentinel-5P TROPOMI) was utilized for technical purposes to estimate anthropogenic emissions and design air pollution abatement strategies. Atmospheric compounds such as NO_2, SO_2, CO, and CH_2O, which are historically and currently being released in large amounts in industrial and urban areas, are of particular interest [8]. Google earth engine (GEE) is a free web-based computing platform developed by Google to facilitate geographical information processing [9]. This cloud-based platform controls an “application programming interface” (API) and a related “interactive development environment” (IDE) that support the algorithms, rapid modeling, and visualization [10]. The Google Earth Engine is also the most widely used platform for handling very large repositories of spectral satellite images and other environmental et al., 2023). The use of GEE for various remote sensing applications such as wetland delineation [11-12], LULC extraction [13-15], and crop mapping [16-19] has become prevalent in recent years. Additionally, GEE utilized for air quality monitoring and assessment [20-23]. Therefore, the main objective of the present investigation is to monitor the spatio-temporal analysis of air quality over Sohag Governorate, Egypt in six ssucssive years viz., 2019, 2020, 2021, 2022, 2023 and 2024 by integrating google earth engine (GEE) and GIS. This provides a more detailed and accurate picture of air quality in the study area, which can help to improve public health and environmental outcomes.

2. Experimental

Study site

The study area covers a part (alluvial plain) of Sohag governorate, Egypt which extending from the northern edge of Qena Governorate at latitude 26° 07′ N to the southern edge of Assiut Governorate at latitude 26°57′ N. It is bounded between longitudes 31°20′ and 32°14′ E (Fig. 1). The study area belongs to the arid region of North Africa,

* Corresponding author E-mail: a_mustafa32@agr.sohag.edu.eg Print ISSN 3062-5513 Online ISSN 3062-5521

which is generally characterized by hot summer and mild winter with low rainfall. Air temperature ranges between 36.5°C (summer) and 15.5°C (Winter), relative humidity ranges between 51% and 61% (Winter), 33% and 41% (Spring), and 35% and 42% (Summer). Rainfall is generally rare and randomly precipitated over the area.

According to the study of Selmy et al. [24], Sohag Governorate mainly includes four classes of different land-uses viz., urban areas (12.3%), water bodies (3.4%), cultivated soils (60.7%) and bare soils (23.6%) as described in table (1).

Table 1: The description of different land-uses of the study area.

Land-uses/Classes	Description
Waterbodies	Nile River, canals, drainage patterns and waste water treatment plants.
Desert lands	Eastern and Western parts of Nile Valley.
Cultivated lands	Cultivated lands in the Nile Valley and Lands under reclamation.
Urban areas	Urban and rural residential, services, commercial, industrial, and roads.

Collect data

In current study, the annually satellite image data of Sentinel-5P for four major pollutants viz., sulfur dioxide (SO_2), nitrogen dioxide (NO_2), ozone (O_3) and carbon mono (CO) products from the GEE. European Space Agency datasets obtained from the Copernicus Sentinel-5 Precursor satellite mission were used as initial data on the content of various pollutants in the atmosphere.

The Sentinel-5 mission consists of a high-resolution spectrometer system that operates within the ultraviolet to shortwave infrared range, utilizing seven distinct spectral bands: UV-1 (270–300 nm), UV-2 (300–370 nm), VIS (370–500 nm), NIR-1 (685–710 nm), NIR-2 (745–773 nm), SWIR-1 (1590–1675 nm), and SWIR-3 (2305–2385 nm). The instrument will be hosted on the MetOp-SG A satellite. To simplify the procedure for obtaining data from the Copernicus Sentinel-5 Precursor satellite (simplification of data processing of netCDF files), the Google Earth Engine (GEE) was used to calculate annual average concentrations of SO_2, NO_2, O_3, CH_4, CH_2O and CO. Comprising a cloud-based computing platform for analyzing and processing large-scale geospatial data, GEE provides a powerful and flexible environment for working with a wide range of remote-sensing, satellite, and other geospatial datasets, including Sentinel-5 Precursor data. One of the key advantages of using GEE for geospatial analysis consists in its ability to efficiently process and analyze huge amounts of data without the need for expensive computing equipment or software. GEE also offers a collaborative environment for sharing data, code, and analysis results with others. The "Sentinel-5P L3" collection was used to estimate the concentration of pollutants (for example, for nitrogendioxide. Image Collection (COPERNICUS/S5P/OFFL/L3_NO$_2$)). For the collection, various methods of filtering (obtaining average annual and monthly values) and data processing (cropping along the boundaries of the studied area) and further analysis of the resulting raster values of pollutants were used. The categories and corresponding concentrations for the studied pollutants are shown in the table (2) as elaborated by EPA, 2009[25].

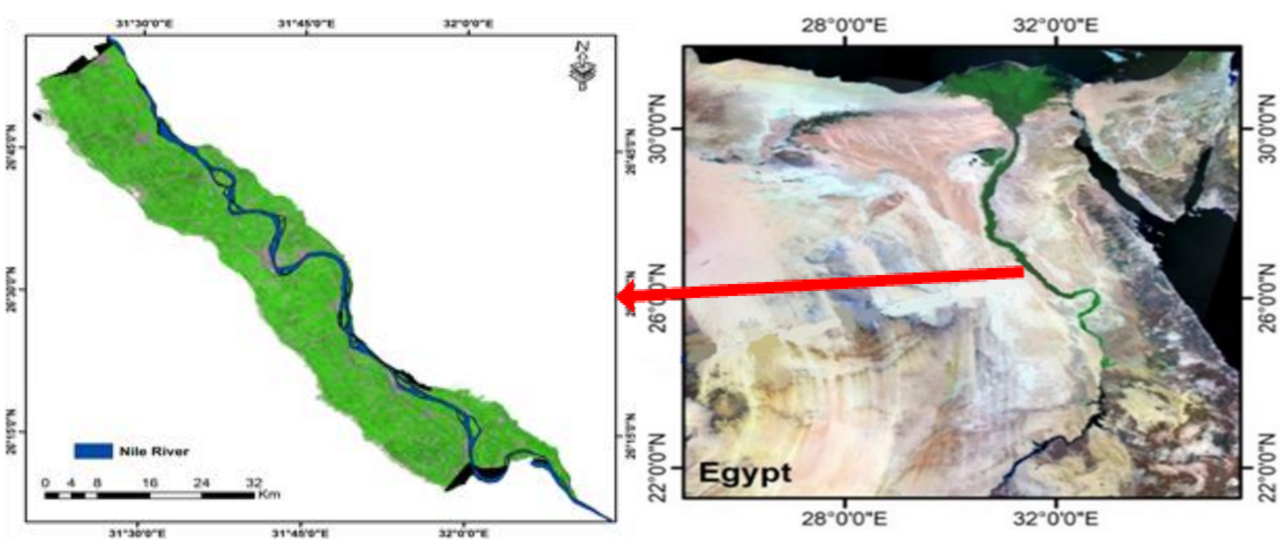

Fig. 1: Location map of the studied area

Table 2: The categories and corresponding concentrations for the studied pollutants

CO (ppm)	O_3 (ppb)	SO_2 (ppb)	NO_2 (ppb)	category
0-4.4	0-54	0-35	0-53	Good
4.5-9.4	55-70	36-75	54-100	Moderate
9.5-124	71-85	76-185	101-360	Unhealthy for sensitive group
12.5-15.4	86-105	186-304	361-649	Unhealthy
15.5-30.4	106-200	305-604	650-1249	Very unhealthy
30.5-50.4	201-604	605-1004	1250-2049	Hazardous

3. Results and discussion:

3.1. Carbon monoxide (CO) concentrations:

Addressing the challenge of CO emission into the atmosphere, through incomplete combustion of compounds such as gasoline, natural gas, oil, coal, and wood in addition to traffic emissions, industrial production, and biomass burning [26]. In the studied period, the CO concentrations varied from 28 to 32 ppm. It was an increase in CO concentrations during 2021 and 2024, whereas, nearly constant concentrations were observed from 2019 until 2022 (figure 2 and table 3). High CO concentration is normally related to locality and population density [27]. In addition, the high CO concentration may be due to the anthropogenic activities as well as the emissions from vehicles and where many power plants and industries are located [28]. The highest concentrations of CO were found around the big cities, main roads and in the south part of the studied area. According to WHO, the CO levels could be described as very unhealthy to hazardous effects.

Table 3: Annual maximum and minimum concentrations of major air pollutants over the study area

Year	CO (ppm)	O_3 (ppb)	NO_2 (ppb)	SO_2 (ppb)
2019	29-31	195-197	104-119	63-438
2020	30-31	201-202	101-118	81-490
2021	30-32	201-203	101-118	64-428
2022	28-29	204-206	107-129	60-416
2023	29-30	201-203	114-137	52-441
2024	30-32	200-209	111-140	57-445

3.2. Ozone (O_3) concentrations:

Ozone is a major greenhouse gas; thus, it plays an important role in both weather and climate, and its impact varies from global to regional scales [29]. While it represents only 0.0012% of the atmospheric composition, ozone acts as an absorber for the energetic particle from the solar ultraviolet radiation (UV), protecting the earth from harmful radiation [30], which has a harmful effect on human health particularly on the skin [31]. The observed increase in UV radiation at the earth's surface has been due to the decrease of amount of ozone at the stratospheric atmospheric layer [32], which is caused by photochemical losses related to anthropogenic reasons [33-34].

Ozone production results from the photochemical reaction of two primary pollutants viz., NOx (NO and NO_2) and hydrocarbons from industry, traffic, vegetation, and biomassburning. During the night, ozone is destroyed by NO emitted by local sources and by deposition to the ground.

In the current investigation, the O3 concentrations during the studied period (table 3 and figure 3) ranged from 195 to 209 ppb. The extremely high concentrations of O3 in the ambient urban air of the study area as might be anticipated. According to WHO, the levels of O3 concentration are described as very unhealthy to hazardous categories.

3.3. Nitrogen oxide (NO_2) concentrations:

NO_2 is a toxic air pollutant that causes severe health impacts and premature death, and it is responsible for tens of deaths annually in Cairo, making it a major health risk in urban and industrial areas. The concentrations of NO_2 ranged from 101 to 140 ppb (figure 3), which means that the NO_2 levels varied between unhealthy for sensitive groups. The presence of this pollutant is closely linked to transportation emissions and heating demands this result aligns with the observation of Hereher et al. [1], which explains its higher concentrations in densely populated areas with high population density. The amount of NO_2 in the atmosphere is linked to several emission sources, such as vehicular emissions and natural sources. The highest concentrations were observed nearby the bigger cities such as Tema, Tahta, Gyhena, Sohag and Alminshah.

3.4. Sulfur dioxide (SO_2) concentrations:

SO_2 gas concentrations in the study area's troposphere, it is primarily associated with industrial and power generation facilities and population density. This pattern is particularly noticeable where significant textile, smelting, chemical, petroleum industries, and electricity generation plants are located. These industrial operations predominantly utilize high sulfur heavy fuel, resulting in the emission of SO_2 and making the region a prominent hotspot for SO_2 emissions [22].

While the majority of SO_2 concentration is attributed to emissions from specific industrial activities in the study area, surprisingly, some residential areas also experience relatively high levels of SO_2. The reason behind these unusually high concentrations of SO_2 in the new urban communities is primarily the extensive use of diesel-fueled trucks for constructing new asphalt roads and carrying out construction activities [22]. Accordingly, the annual concentrations of SO_2 during the studied period ranged from 52 to 490 ppb which indicated that the categories varied from moderate to unhealthy as shown in figure (5). As appears in figure (5), the highest concentration of SO_2 were found around the bigger cities in the study area and heavy populated area.

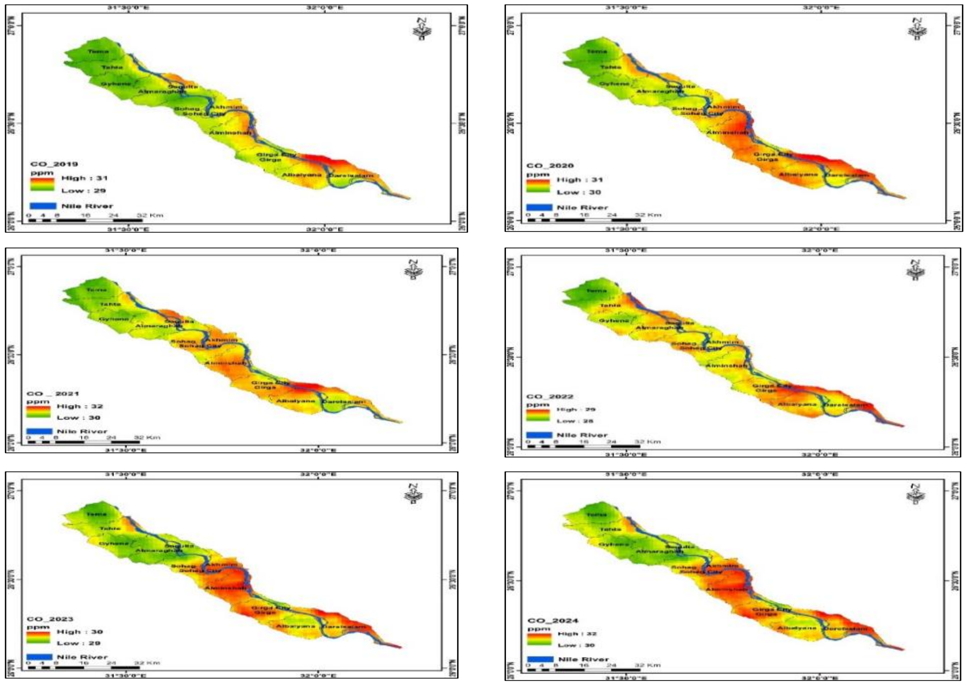

Fig. 2: The distribution of CO in the study area for the period 2019 to 2024.

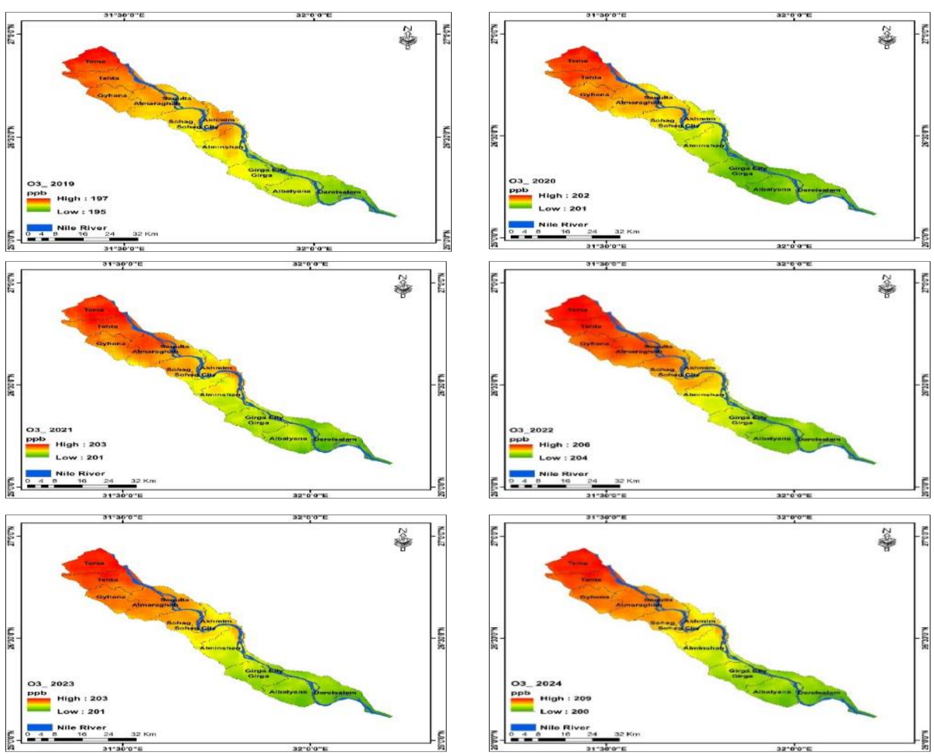

Fig. 3: The distribution of O_3 in the study area for the period 2019 to 2024.

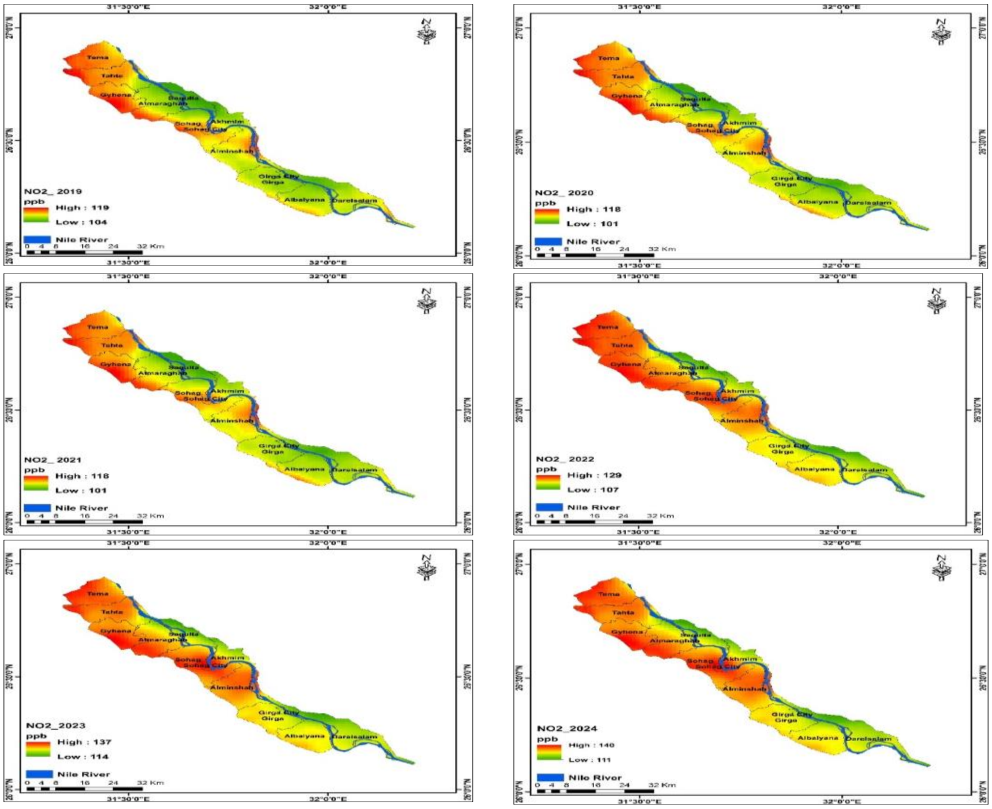

Fig. 4: The distribution of NO_2 in the study area for the period 2019 to 2024.

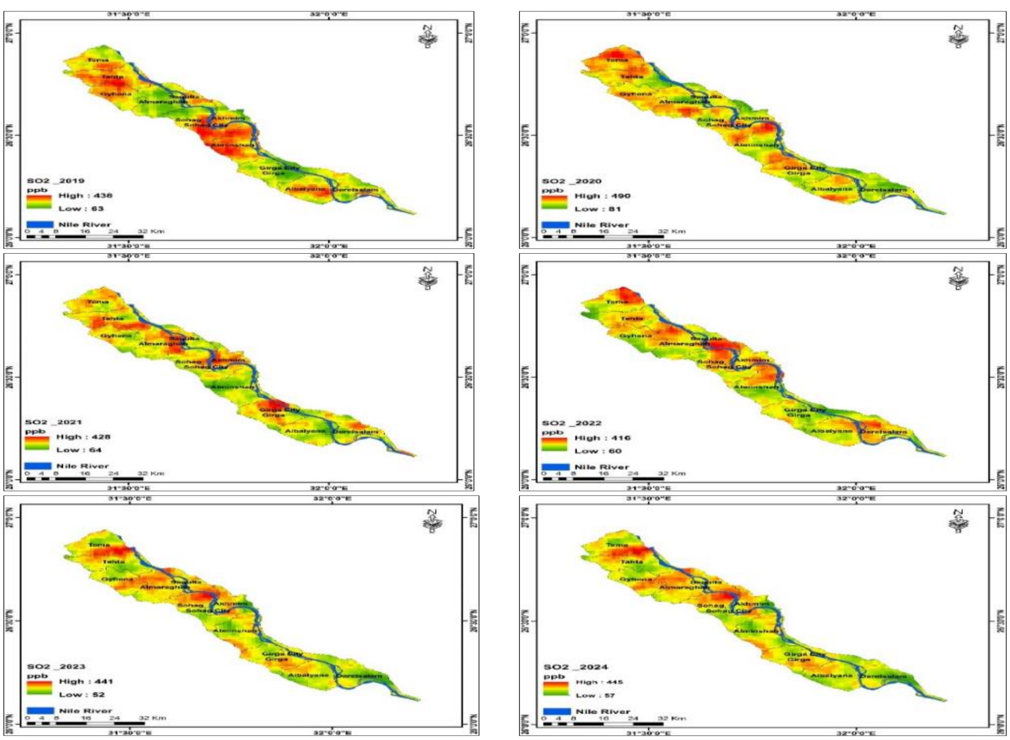

Fig. 5: The distribution of SO_2 in the study area for the period 2019 to 2024.

4. Conclusion

Air pollution represents one of the major environmental stressors with serious implications on human health and ecosystem balance. Recently remote sensing imageries as an alternative cost and time-effective method compared with regular monitoring techniques were used for provision of appropriate data concerning air quality over large areas. In this context, Sentinel-5P satellite provides high-resolution images of atmospheric pollutants including nitrogen dioxide (NO_2), ozone (O_3), carbon monoxide (CO) and sulfur dioxide (SO_2). The obtained results showed high variation in the concentration of CO, O_3, NO_2 and SO_2, in the study area due to the primary sources of air pollution in the study area including basically industry, urbanization and transportation. Furthermore, the results demonstrated that the study area is subjected to high emissions of air pollutants primarily due to industry and traffic. Additionally, the uncontrolled urban expansion of the urban centers causes frequent air pollution issues. The results revealed the excellence of satellites in detection of air pollutants in the study area due to almost daily global coverage. Additionally, the satellite data provides superior spatial distribution of the aerosols, which is considered difficult to measure from ground observations especially during storm events. Furthermore, there is a lack of ground measurements as it is not feasible to put a dense ground monitoring network to assess and monitor surface air quality. Even Though, air pollutants measurements using satellite data have some uncertainty, but satellite data can serve as surrogate to measure the surface level of air quality. Therefore, it is crucial to understand the uncertainties associated with satellite data. We highly recommend that users must pay attention to the quality flags and density of the data for a specific region.

5. References

[1] M. Hereher, R. Eissa, A. Alqasemi and A.M. El Kenawy, "Assessment of air pollution at Greater Cairo in relation to thespatial variability of surface urban heat island", Environ. Sci.Pollut. Res., vol., pp 29, 21412-21425, 2022.

https://doi.org/10.1007/s11356-021-17383-9.

[2] H. Wen, H, P. Nie, M. Liu, R. Peng, T. Guo, C. Wang and X. Xie," Multi-health effects of clean residential heating: evidencesfrom rural China's coal-to-gas/electricity project", EnergySustain, Dev., vol 73, pp 66-75,2023.

[3] M.K. Mostafa, G. Gamal and A. Wafiq," The impact of COVID19 on air pollution levels and other environmental indicators-A case study of Egypt", J. Environ. Manag. Vol.277, pp. 111496, 2021.

[4] IPCC, 2021. Contribution of Working Groups I, II and III to theSixth Assessment Report of the Intergovernmental Panel onClimate Change. https://www.ipcc.ch/report/ar6/wg1/.

[5] Q. Liu, D. Yang and L. Cao, "Evolution and prediction of thecoupling coordination degree of productionelivingeeco-logical space based on land use dynamics in the daqing riverbasin", China. Sustainability, vol. 14, pp. 10864, 2022.

[6] F. Nouri, M. Taheri, M. Ziaddini, J. Najafian, K. Rabiei and A. Pourmoghadas, "Effects of sulfur dioxide andparticulate matter pollution on hospital admissions for hy-pertensive cardiovascular disease: a time series analysis', Front. Physiol., vol. 14, pp. 1124967, 2023.

[7] J. Hwang, K. Maharjan and H. Cho, "A review of hydrogenutilization in power generation and transportation sectors: achievements and future challenges", Int. J. Hydrogen Energy, vol. 48 (74), pp. 28629e28648, 2023.

[8] E.W Nyaga.," Aerosol Remote Sensing and Modelling: Estimation of Vehicular Emission Impact on Air Pollution inNairobi', University of Nairobi, Kenya, 2021.

[9] N. Gorelick, M. Hancher, M. Dixon, S. Ilyushchenko, D. Thau, R. Moore, "Google Earth Engine: Planetary-scale geospatial analysis for everyone", Remote sensing of Environment, vol. 202, pp. 18-27, 2017.

[10] P. Pérez-Cutillas, A. Pérez-Navarro, C. Conesa-García, D. A. Zema and J. P. Amado-Álvarez," What is going on within google earth engine? A systematic review and meta-analysis", Remote sensing applications: Society and environment, vol. 29, pp. 100907, 2023.

[11] M. Amani, B. Brisco, M. Afshar, S. M. Mirmazloumi, S. Mahdavi, S. M. J. Mirzadeh, W. Hung and J. Granger, "A generalized supervised classification scheme to produce provincial wetland inventory maps: An application of Google Earth Engine for big geo data processing", Big Earth Data, vol. 3(4), pp. 378-394, 2019.

[12] M. Mahdianpari, H. Jafarzadeh, J. E. Granger, F. Mohammadimanesh, B. Brisco, B. Salehi, Q and Weng, "A large-scale change monitoring of wetlands using time series Landsat imagery on Google Earth Engine: a case study in Newfoundland", GIScience & Remote Sensing, vol. 57(8), pp. 1102–1124,2020. https://doi.org/10.1080/15481603.2020.1846948.

[13] H. A. Zurqani, C. J. Post, E. A. Mikhailova, M. A. Schlautman, and J. L. Sharp, "Geospatial analysis of land use change in the Savannah River Basin using Google Earth Engine", International journal of applied earth observation and geoinformation, vol. 69, pp. 175-185, 2018.

[14] A. Ghorbanian, M. Kakooei, M. Amani, S. Mahdavi, A. Mohammadzadeh and M. Hasanlou," Improved land cover map of Iran using Sentinel imagery within Google Earth Engine and a novel automatic workflow for land

cover classification using migrated training samples", ISPRS Journal of Photogrammetry and Remote Sensing, vol. 167, pp. 276-288, 2020.

[15] E. A. Abdelsamie, A. R. A. Mustafa, A. S. El-Sorogy, H. F. Maswada, S. A. Almadani, M. S. Shokr and Meroño de Larriva, "Current and Potential Land Use/Land Cover (LULC) Scenarios in Dry Lands Using a CA-Markov Simulation Model and the Classification and Regression Tree (CART) Method: A Cloud-Based Google Earth Engine (GEE) Approach", Sustainability, vol. 16(24), pp. 11130, 2024.

[16] J. Xiong, P.S. Thenkabail, M.K. Gumma, P. Teluguntla, J. Poehnelt, R.G. Congalton, K. Yadav and D. Thau, "Automated cropland mapping of continental Africa using Google Earth Engine cloud computing", ISPRS Journal of Photogrammetry and Remote Sensing, vol. 126, pp. 225-244, 2017.

[17] A. J. Oliphant, P. S. Thenkabail, P. Teluguntla, J. Xiong, M. K. Gumma, R. G. Congalton and K. Yadav," Mapping cropland extent of Southeast and Northeast Asia using multi-year time-series Landsat 30-m data using a random forest classifier on the Google Earth Engine Cloud", International Journal of Applied Earth Observation and Geoinformation, vol. 81, pp. 110-124, 2019.

[18] S. Xie, L. Liu, X. Zhang, J. Yang, X. Chen and Y. Gao, "Automatic land-cover mapping using landsat time-series data based on google earth engine", Remote sensing, vol. 11(24), pp. 3023, 2019.

[19] M.K. Gumma, P.S. Thenkabail, P.G. Teluguntla, A. Oliphant, J. Xiong, C. Giri, V. Pyla, S. Dixit and A.M. Whitbread, "Agricultural cropland extent and areas of South Asia derived using Landsat satellite 30-m time-series big-data using random forest machine learning algorithms on the Google Earth Engine cloud", GIScience & Remote Sensing, vol. 57(3), pp.302-322, 2020.

[20] Y. Meng, M. S. Wong, H. Xing, M. P. Kwan, and Zhu, R.," Yearly and daily relationship assessment between air pollution and early-stage COVID-19 incidence: Evidence from 231 countries and regions", ISPRS International Journal of Geo-Information, vol. 10(6), pp. 401, 2021.

[21] F. Ghasempour, A. Sekertekin and S. H. Kutoglu, "Google Earth Engine based spatio-temporal analysis of air pollutants before and during the first wave COVID-19 outbreak over Turkey via remote sensing", Journal of Cleaner Production, vol. 319, pp. 128599, 2021.

[22] S. Sameh, F. Zarzoura and M. El-Mewafi, "Spatio-temporal Analysis Mapping of Air Quality Monitoring in Cairo using Sentinel-5 satellite data and Google earth engine", Mansoura Engineering Journal, vol. 49(1), pp. 3, 2023.

[23] B. Halder, I. Ahmadianfar, S. Heddam, Z.H. Mussa, L. Goliatt, M.L. Tan, Z. Sa'adi, Z. Al-Khafaji, N. Al-Ansari, A.H. Jawad, and Z.M. Yaseen," Machine learning-based country-level annual air pollutants exploration using Sentinel-5P and Google Earth Engine", Scientific Reports, vol. 13(1), pp.7968, 2023.

[24] S.A. Selmy, D.E. Kucher, G. Mozgeris, A.R. Moursy, R. Jimenez-Ballesta, O.D. Kucher, M.E. Fadl and A. -r.A.J.R. S Mustafa," Detecting, analyzing, and predicting land use/land cover (LULC) changes in arid regions using landsat images, CA-Markov hybrid model, and GIS techniques", vol. 15, pp. 5522, 2023.

[25] EPA (United States Environmental Protection Agency), "Technical assistance document for reporting of daily air quality-the air quality index (AQI)", EPA-454/B-09-001. U.S., Environmental Protection Agency, North Carolina, 2009.

[26] T. Borsdorff, H. Hu, O. Hasekamp, R. Sussmann, M. Rettinger, F. Hase, J. Gross, M. Schneider, O. Garcia, W. Stremme, and M. Grutter," Mapping carbon monoxide pollution from space down to city scales with daily global coverage", Atmospheric Measurement Techniques, vol. 11(10), pp.5507-5518, 2018.

[27] M. Filonchyk and M. Peterson," Air quality changes in Shanghai, China, and the surrounding urban agglomeration during the COVID-19 lockdown", Journal of Geovisualization and Spatial Analysis, vol. 4(2), pp. 22, 2020.

[28] G. Gamal, O. M. Abdeldayem, H. Elattar, S. Hendy, M. E. Gabr and M. K. Mostafa, "Remote sensing surveillance of NO_2, SO_2, CO, and AOD along the Suez Canal Pre-and Post-COVID-19 lockdown periods and during the blockage", Sustainability, vol. 15(12), pp. 9362, 2023.

[29] M. Rex, R.J.P.von der Salawitch, N.R. Gathen, P. Harris, M. Chipperfield and B. Naujokat," Arctic ozone loss and climate change", Geophys. Res. Lett., vol. 31, pp. L04116, 2004. [Google Scholar] [CrossRef].

[30] D. Alexandris, C. Varotsos, K.Y. Kondratyev and G. Chronopoulos," On the altitude dependence of solar effective UV", Phys. Chem. Earth Part C Sol. Terr. Planet. Sci., vol. 24, pp. 515–517, 1999. [Google Scholar] [CrossRef].

[31] World Health Organization (WHO). Protection Against Exposure to Ultraviolet Radiation; Technical Report WHO/EHG #17; WHO: Geneva, Switzerland, 1995. [Google Scholar].

[32] V.E. Fioletov, L. McArthur, J.E. Kerr and D.I. Wardle, "Long-term variations of UV-Birradiance over Canada estimated from Brewer observations and derived from ozone and pyranometer measurements", J. Geophys. Res.,

vol. 106, pp. 2307–2309, 2001. [Google Scholar] [CrossRef].

[33] N.R.P. Harris, J. Ancellet, L. Bishop, D.J. Hofmann, J.B. Kerr, R.D. McPeters, W.J. Prendez, J. Randel, B.H. Staehelin and A. Subbaraya, “Trends in stratospheric and free tropospheric ozone”, J. Geophys. Res., vol. 102, pp. 1571–1590, 1997. [Google Scholar] [CrossRef].

[34] World Meteorological Organization (WMO). Scientific Assessment of Ozone Depletion: Global Ozone Research and Monitoring Project; Technical Report 50; WMO: Geneva, Switzerland, 2006. [Google Scholar].

Journal of sustainable food, water, energy and environment

Effect of climate change on Spodoptera frugiperda (J.E. Smith) (Lepidoptera: Noctuidae), the new pest has been detected in Egypt

Hany Ahmed Fouad and Abdelalem Saad Soliman Desoky

Plant Protection Department, Faculty of Agriculture, Sohag University, Egypt.

Received: 8 Jan. 2025, Revised: 22 Jan. 2025, Accepted: 4 Feb. 2025 Published online: 1 Apr. 2025

Abstract: The fall armyworm (FAW) is of tropical–subtropical origin and defined as one of the most destructive agricultural pests globally, including Egypt. This study aims to effect of temperature factor on the biological cycle and generations of Spodoptera frugiperda under laboratory conditions. The highest mortality occurred when the caterpillars were kept at 32°C in the F2 generation. In general, among the temperatures tested, 24 °C and 28 °C promoted the greatest number of days in incubation. The average duration of insect development in days was inversely proportional to the increase in temperature. Understanding the climate factors are necessary to clarify the possible influences of global climate change, including warming on this species, in addition to evaluating the adaptation of insects over generations.

Keywords: Spodoptera frugiperda; climate change; global worming

1. Introduction

The fall armyworm (FAW), Spodoptera frugiperda (J. E. Smith, 1797), known as an important agricultural pest around the world, including Egypt. It is indigenous to the tropical–subtropical regions in the Western Hemisphere, although its distribution has expanded over large parts of America, Africa, Asia and Oceania in the last few years. Global climate change may significantly impact the geographic distribution of biodiversity, alter biodiversity, and affect interactions between species and ecosystems [1]. Temperature is one of the abiotic factors that exerts great influence on insect biology and this factor can affect the duration of the life cycle, population density, size and genetic composition, the extent of host plant exploitation, as well as local and geographic distribution linked to colonization and extinction [2].

insects are ectotherms, exhibiting a high degree of sensitivity to ambient temperature in their physiological processes. Several pieces of evidence indicate that not only higher temperatures, but also greater climate variability can have a significant effect on organisms and ecosystems [3]. Species present individual responses to temperature, carbon dioxide concentration, and other environmental factors, thus, climate change may affect the temporal and spatial association between species that interact at different trophic levels [4].

Several efforts have reported that temperature directly or indirectly influences the geographic distribution, phenology and natural enemies of the FAW, and thus may affect the damage to crops, e.g., the increased developmental rate accelerates the intake of crops at higher temperatures. Under some extreme temperatures, the FAW is likely to regulate various genes expression in response to environmental changes, which causes a wider viability and possibility of invasion threat. Therefore, this paper seeks to review and critically consider the variations of developmental indicators, the relationships between the FAW and its natural enemies and the temperature tolerance throughout its developmental stage at varying levels of heat/cold stress.

Based on this, the study of adaptation to certain thermal conditions is relevant to discussions about the effect of global warming on the distribution and abundance of ectothermic animals [5]. Climate change can affect herbivorous insects directly, through impacts on their physiology and behavior, or indirectly, where insects respond to climate-induced changes mediated by other factors, such as the host plant [2]. Thus, considering the importance of temperature for insect development and the possible increase in the occurrence of S. frugiperda in soybeans, this study aimed to evaluate the influence of different temperatures on the biological aspects of this insect over four generations.

2. Material and methods

The experiments were carried out in the laboratory of Entomology, Plant Protection Department, Faculty of Agriculture, Sohag University, Egypt. The maize plants offered to the insects were sown in five-liter pots, with five plants per pot putted in a growth room with a 14-hour photoperiod, temperature of 28 °C and relative humidity of 65 %.

Insect biology was performed in a B.O.D. rearing chamber at different temperatures (24°C, 28°C, 32°C and 36°C), throughout the insect biology period, to represent the

* Corresponding author E-mail: abdelalem2011@gmail.com Print ISSN 3062-5513 Online ISSN 3062-5521

daily oscillation, with humidity of 70 ± 10% and a 14-h photophase. Second-instar S. frugiperda larvae from the mass rearing in the laboratory, reared from hatching on maize leaves and at their respective temperatures, were individualized in paraffin cups with plastic lids. The larvae were evaluated daily, observing mortality and development time of each stage. The food was replaced daily.

After reaching the pupal stage, these were separated by sex and, immediately after emergence, the adults were placed in individual cages made of PVC tubes, 20 cm high by 10 cm in diameter [6]. For oviposition and egg collection, the cage was lined internally with A4 paper, which was removed whenever egg laying was observed. The individualized couples were kept at the same temperature to ensure continuity of generations. The cages with the adult couples were observed daily, replacing the food and recording mortality in each replicate.

For the biology of the insects, considering the larval stage to the pupal stage, and for the evaluation of adult longevity, a completely randomized design with 60 replicates was used. The response variables considered in this study were: caterpillar mortality (%) and development time (days).

Statistical analysis

Mortality and development time were analyzed using analysis of variance (ANOVA) with Tukey mean tests at a 5% probability level using the SAS-Statistical Analysis System, version 9.2 (2009) statistical program [7].

3. Results and discussions

Under the conditions of global climate change, including warming, the distribution range of S. frugiperda is expected to significantly increase [8-9]. In general, the different temperatures affected the biological aspects of S. frugiperda. The analysis of variance (ANOVA) (p>0.05) indicated differences in the percentage of mortality according to the treatments (Table 1). The highest mortality occurred when the caterpillars were kept at 32°C in the F2 generation.

At this same temperature, when the generations were compared, an increase in mortality was observed. In the F0 generation, significant difference was observed in mortality in insects kept at the different temperatures adopted. At a temperature of 24°C, the highest mortality was also observed in the F1 and F2 generation.

Table 2 shows the incubation and development period of insects at different temperatures, from the egg to hatching, which did not present variability between the data for the application of the average test. In general, among the temperatures tested, 24 °C and 28 °C promoted the greatest number of days in incubation.

The larval development time of the insects were influenced by the temperatures (Table 2). The average duration of insect development in days was inversely proportional to the increase in temperature, with the longest duration observed at 24°C and the shortest duration at 36°C (F0). This fact was also observed in the F1, F2 and F3 generations at temperatures of 24°C and 33°C. At a temperature of 33°C, a difference was observed between the generations, with the longest development time in the F0 generation. Ali et al. [10] reported the development rate of larvae at temperatures ranging between 21 and 33 oC to increase linearly and, therefore, regarded the temperature range between 21 and 33 °C to be suitable for S. frugiperda development.

In the pupal stage, the average duration, in days, within the F0 and F1 generations was longer at the temperature of 24°C, with no difference in the F2 and F3 generations at the temperatures of 25°C, 28°C and 32°C. Within the temperatures of 24°C, 28°C and 32°C in (F0) a greater number of days in the pupal stage, with no significant difference, was observed when compared to the other generations. The S. frugiperda pupal development time 8.25 days (32 oC), which is in a similar range (6.6 days at 32 oC) to that reported by Busato et al. [11]. Under future climate scenarios, it is observed a reduction in the time to complete the life cycle, as representative scenarios become stronger relative to reference period [12].

Table 1: Percentage of mortality (±S.E.) of Spodoptera frugiperda reared on maize leaves subjected to different temperatures, for four generations, there were no survivors.

Generation	**Temperature**				**F value**	***P* value**	**L.S.D**
	24 ºC	**28 ºC**	**32 ºC**	**36 ºC**			
F0	20.91±0.32	16.38±0.05	24.14±0.29	29.29±0.02	603.25	<.0001	1.0026
F1	31.63±0.61	26.45±0.28	32.13±0.40	-	48.87	0.0002	1.954
F2	31.46±0.02	28.18±0.64	50.79±1.28	-	219.55	<.0001	3.578
F3	28.26±0.91	24.90±0.57	43.49±1.14	-	119.67	<.0001	3.9298
F value	64.84	410.01	175.84				
***P* value**	<.0001	<.0001	<.0001				
L.S.D	2.8204	1.1865	4.04				

Table 2.: The mean development time (days ±S.E.) of different life stages of Spodoptera frugiperda subjected to different temperatures, for four generations The different among averages in a row or column by the Tukey test at a 5% probability level, there were no survivors.

Generation	Temperature				F value	*P* value	L.S.D
	24 ºC	28 ºC	32 ºC	36 ºC			
Egg							
F0	2.33±0.33	2.00±0	1.67± 0.33	1.33±0.33	2.22	0.16	1.3074
F1	2.33±0.33	2.00±0	1.67±0.33	-	1.50	0.30	1.1809
F2	2.67±0.33	2.00±0	1.67±0.33	-	3.50	0.1	1.1809
F3	3.00±0.58	2.67±0.33	2.00±0.58	-	1.00	0.42	2.2093
F value	0.61	4.00	0.17				
***P* value**	0.6265	0.0519	0.9159				
L.S.D	1.8489	0.7548	1.8489				
Larva							
F0	20.22±0.45	18.67±0.66	16.19±0.48	12.71±0.27	45.48	<.0001	2.1992
F1	18.63±0.31	16.46±0.12	12.88±0.35	-	107.72	<.0001	1.2154
F2	17.47±0.22	15.26±0.27	14.97±0	-	45.81	0.0002	0.8748
F3	19.73±0.17	16.33±0.31	14.99±0.53	-	43.87	0.0003	1.6005
F value	16.21	13.00	11.90				
***P* value**	0.0009	0.002	0.003				
L.S.D	1.3779	1.7946	1.8058				
Pupa							
F0	9.25±0.12	8.26±0.20	8.25±0.11	7.48±0.08	27.91	0.0001	0.6218
F1	9.13±0.22	8.14±0.15	8.21±0.21	-	8.22	0.019	0.8392
F2	8.76±0.30	7.99±0.07	8.07±0.07	-	5.45	0.04	0.7836
F3	8.83±0.09	7.76±0.22	7.96±0.25	-	8.06	0.02	0.8723
F value	1.39	1.57	0.57				
***P* value**	0.3144	0.2711	0.6511				
L.S.D	0.9017	0.7749	0.7989				

4. Conclusion

The fall armyworm is an important agricultural pest of various crops; therefore, areliable method is needed to predict its occurrence in the field. Temperature-dependent development and thermal biology parameters are commonly used methods for simulating insect phenology. Considering the results obtained, it can be suggested that changes in temperature may cause negative effects on populations of S. frugiperda, which may reduce its incidence in the field. However, additional studies on the temperature-insect/plant interaction are necessary to clarify the possible influences of global climate change, including warming on this species, in addition to evaluating the adaptation of insects over generations.

5. References

[1] M.E. Dillon, G. Wang and R.B. Huey,” Global metabolic impacts of recent climate warming”, Nature, vol. 467, PP. 704-706, 2010.

[2] J. S. Bale, G. J. Masters, I. D. Hodkinson, C. Awmack, T. M. Bezemer, V. K. Brown, J. Butterfield, A. Buse, Coul-Son, J. Farrar, J. E. G. Good, R. Harrington, J. C. Hart- S. Ley, T. H. Jones, R. L. Lindroth, M. C. Press, I. Symrni Oudis, A. Watt and J. B. Whittaker, “Herbivory in global climate change research: direct effects of rising temperature on insect herbi- vores”, Global Change Biology, vol. 8(1), pp. 1-16, 2002.

[3] A. Sentis, J.-L. Hemptinne and J. Brodeur,” Effects of simulated heat waves on an experimental plant–herbivore–predator food chain”, Global change biology, vol. 19 (3), pp. 833-842, 2013.

[4] R. Harrington, I. Woiwod and T. Sparks,” Climate change and trophic interactions”, Trends in Ecology & Evolution, vol. 14 (4), pp.146- 150, 1999.

[5] A. F.G. Dixon, A. Honek, P. Keil, M. A. A. Kotela, A. L. Šizling and V. Jarošík,” Relationship between the minimum and maximum tempera- ture thresholds for development in insects”, Functional Ecology, vol. 23, pp. 257-264, 2009.

[6] P. Milano, E. Berti Filho, J. R. P. Parra and F. Cônsoli, L, “Temperature Effects on the Mating Frequency of Anticarsia gemmatalis Hüebner and Spodoptera frugiperda (J.E. Smith) (Lepidoptera: Noctuidae)”, Neotropical Entomology, vol. 37, pp. 528-535, 2008.

[7] SAS Institute, SAS/STAT: User’s Guide: Statistics, Version 9.2. Cary: SAS Institute, NC: Statistical Analysis Systems, 7869p,2009.

[8] R. Wang, C. Jiang, X. Guo, D. Chen, C. You, Y. Zhang, M. Wang and Q. Li, “Potential distribution of Spodoptera frugiperda (JE Smith) in China and the major factors influencing distribution” Glob. Ecol. Conserv. Vol. 21, pp. 865, 2020.

[9] M.N. Baloch, J. Fan, M. Haseeb and R. Zhang, “Mapping potential distribution of Spodoptera frugiperda (Lepidoptera: Noctuidae) in central Asia”, Insects, vol.11, pp. 172, 2020.

[10] A. Ali, R.G. Luttrell and J.C Schneider, “Effects of temperature and larval diet on development of the fall armyworm (Lepidoptera: Noctuidae)”, Ann. Entomol. Soc. Am. Vol. 83, pp. 725-733, 1990.

[11] G.R. Busato, A.D. Grützmacher, M.S. Garcia, F.P. Giolo, M.J. Zotti, J.D.M. Bandeira,” Thermal requirements and estimate of the number of generations of biotypes “corn” and “rice” of Spodoptera frugiperda”, Pesq. Agropec. Bras., vol. 40: 329-335, 2005.

[12] T. C. A. Sumila, S. E. T. Ferraz and A., “Durigon. Climate change impact on Spodoptera frugiperda (Lepidoptera: Noctuidae) life cycle in Mozambique”, PLOS Climate, vol. 18, pp. 1-25, 2023.

Journal of sustainable food, water, energy and environment

Inactivation of Microcystis aeruginosa by undoped and cobalt-doped copper oxide nanoparticles: towards sustainable water treatment

Zakaria A Mohamed[1], Asmaa A Hosny[2], Bahig El-Deeb1, E. M. M. Ibrahim[2]

[1]Department of Botany and Microbiology, Faculty of Science, Sohag University, Sohag, 82524, Egypt.
[2]Physics Department, Faculty of Science, Sohag University, 82524 Sohag, Egypt.

Received: 10 Jan. 2025, Revised: 25 Jan. 2025, Accepted: 7 Feb. 2025 Published online: 1 Apr. 2025

Abstract: One of the major challenges in reducing the risk of cyanobacteria to environmental health is employing safe and effective techniques to treat and remove their cells from water sources. Nano-materials such as copper oxide nanoparticles (CuO NPs) have drawn a lot of interest as a sustainable way to inactivate microorganisms and adsorb contaminants in wastewater because of their catalytic activity, low cost and low cytotoxicity. Herein, we investigated the inhibitory effects of undoped and cobalt-doped copper oxide nanoparticles (Co-CuO NPs) on Microcystis aeruginosa, a common toxic cyanobacterium found in water sources. The results showed that both undoped and Co-doped CuO NPs inactivated M. aeruginosa growth, with doped NPs having a higher effectiveness (100%) than undoped ones (99%) at 25 mg/L. According to regression Probit analysis, the medium effective concentrations (EC50) of these NPs varied with exposure time, reaching their lowest values (0.8 and 0.3 mg/L, respectively) at 96 hours and their greatest values (5.6 and 4.6 mg/L, respectively) at 24 hours. Additionally, the results showed that these NPs can concurrently adsorb microcystin (MC) toxins that are released into the medium upon cell lysis. Since nanoparticles are firmly bound to the surfaces of cyanobacterial cells, they settle as flocs and are easily eliminated with the sludge. Therefore, both undoped and doped CuO NPs could be employed as coagulants in drinking water treatment plants to remove microcystin toxins and cyanobacterial cells at the same time.
Keywords: Microcystis aeruginosa; microcystin; coagulant; Nano-CuO.

1. Introduction

In recent decades, the growing frequency of nutrient enrichment in water bodies, especially nitrogen and phosphorus, coupled with climate change has made cyanobacteria bloom a major environmental concern worldwide [1-3]. One of the most common toxic cyanobacteria species, M. aeruginosa outgrows under eutrophic water bodies and forms harmful blooms, and thus represents a serious threat to the aquatic ecosystem, fishery, tourism industry, and drinking water sources through production of potent toxins called microcystins (MCs) [4-5].

Many strategies including physical, chemical and biological methods have been proposed to control or remove cyanobacterial blooms from water bodies [6-7]. However, physical methods are expensive and time-consuming [8], while biological methods using microorganisms are not specific for killing cyanobacteria but also can destroy other beneficial algae. Additionally, chemical inactivation of cyanobacterial cells (e.g., by $CuSO_4$, as well as Cu^{2+}-based algaecide) is efficient strategy for mitigation of cyanobacteria bloom and widely applied in lakes and reservoirs [9]. However, it affects the integrity of the cyanobacterial cells causing massive cell lysis and release of microcystin toxin in the water, which are hard to be removed by conventional treatment processes [10-11]. Therefore, it is necessary to look for a cost-effective and efficient cyanobacterial inactivator without secondary pollution and toxin release in the natural environment.

Recently, previous investigations have shown that some nanoparticles could efficiently inactivate the growth of algae and cyanobacteria [12-15]. However, the mechanism of all these studies was based on the damage of algae cells, which would induce the release of intracellular compounds including toxins and other substances serves as precursors for disinfection byproducts [16]. Therefore, the ideal inactivating chemical for algae cells should boost the efficiency of algae removal while avoiding cell damage. Among metal oxide nanoparticles, CuO NPs have garnered special attention because of their unique physical and chemical characteristics, as well as their antibacterial, antioxidant, and antifungal qualities, which have allowed them to be used in a wide range of biomedical, industrial, agricultural, electronic, and environmental applications [17-18]. In fact, CuO nanoparticles biosynthesized from plant extracts have advantages over those that are chemically synthesized because the bioactive metabolites in the extracts (such as phenols, flavonoids, carboxylic acids, terpenoids, and tannins) can influence the physico-chemical properties, stability, and toxicity of the nanoparticles, as well as

* Corresponding author E-mail: mzakaria_99@yahoo.com Print ISSN 3062-5513 Online ISSN 3062-5521

enhance their affectivity and biocompatibility [19- 21]. Therefore, the present study aimed to investigate the ability of biosynthesized CuO and Co-doped CuO nanoparticles to inactivate the growth of M. aeruginosa and eliminate microcystin toxins.

2. Materials and Methods

2.1 Culturing of Microcystis aeruginosa

Microcystis aeruginosa used in the experiments was obtained from from culture collection at Department of Botany & Microbiology, Sohag University, Egypt. This cyanobacterium was originally isolated from freshwater fishpond and found to produce three MC variants (MC-LR, -RR, -YR), with cell quota of 160,140 and 58 pg cell-1, respectively [22]. M. aeruginosa was grown in BG-11 medium at 25˚C under cool white fluorescent lights at an intensity of 50 μmol m−2 s−1 (14h light/10h dark) for 14 days (i.e., the exponential growth phase). The cells were harvested at exponential stage (cell density=2.1 ×107 cells mL−1) and centrifuged at 6000 x g for 15 min.

2.2 CuO nanoparticles

Both undoped and doped nanoparticles used in our adsorption experiments were obtained from Biophysics laboratory, Physics department, Sohag University. These nanoparticles were previously biosynthesized using sugarcane juice [23] and characterized by the following features. CuO and 9% Co-doped CuO nanoparticles are composed of roughly spherical particles with average size of 9.3 and 13nm, respectively. The X-ray diffraction (XRD) pattern of these biosynthesized nanoparticles showed their highly crystalline structure with average crystallite size of 11.8 and 8.3 nm, respectively.

FTIR spectra for ZnO NPs showed broadband at ~3409, 2079, 1632, and 694 cm-1, corresponding to vibration hydroxyl group O-H, the isothiocyanate stretching C=O, stretching amide group, C=N, and characteristic ZnO stretching, respectively .FTIR spectra for CuO and Co-doped CuO nanoparticles showed broadband at 3290, 1639, 1060, and 586 cm-1, corresponding to hydroxyl group O-H, C=O stretch group, O-C=O, and bending vibration =C–H, respectively. Stock solution of CuO and Co-doped CuO nanoparticles was prepared in deionized water, and dispersed by sonication for 45 min at 40 Hz, using Probe sonicator (Q-500, Qsonica, USA). From the stock solution, working solutions were made in BG-11 medium for cell removal experiments.

2.3 Growth inhibition of Microcystis aeruginosa by nanoparticles

This experiment was conducted in 1000 ml- beakers containing BG-11 medium (pH8, close to that of the natural freshwater), exponentially growing cells of M. aeruginosa (initial cell density= 1x107 cells/mL) and different concentrations of either CuO or Co-doped CuO nanoparticles (5,10, 20 and 25 mg/L). Beakers containing only BG-11 medium and M. aeruginosa cells but without nanoparticles were used as controls. Both control and treated cultures were incubated for 96 hours at the same conditions as described above in Culturing of Microcystis aeruginosa section, while stirred by a magnetic stirrer at 250 rpm to simulate turbulence in natural water bodies. Cell densities were counted every 24 h using hemocytometer under light microscope. The algae growth inhibition rate (%) was calculated according to the following equation

$$\text{Growth Inhibition}(\%) = \frac{C_0 - C_t}{C_0} \times 100$$

where C0 and Ct are the cell number (cells/mL) at 0 h and t h, respectively. The inactivation efficiencies were evaluated as medium effective concentration (EC50), which was determined using Probit regression analysis in Excel software.

To study the potential release of microcystin toxin into the medium under the effect of CuO nanoparticles, an aliquot of control and treated cultures was aseptically drawn every 24 hours. The samples were filtered via GF/C filters, and microcystin concentrations were then determined directly in the filtrate using ELISA kits (Abraxis, Warminster, PA, USA) according to Carmichael and An et. al. [24]

2.4 Statistical analysis

The differences in removal percentages of cyanobacterial cells and microcytsin concentrations between treated and control groups were estimated by One-way Analysis of Variance (ANOVA) ($P < 0.05$) using SPSS 22.0 (SPSS Inc., USA). All Data were expressed as average ± standard deviation.

3. Results and discussions

The results of the present study shown in Fig.1A and B, showed that the growth inhibition rate of M. aeruginosa increased gradually with increasing the concentrations of either pure CuO NPs or Co-doped CuO NPs, and with the exposure time as well. Undoped CuO NPs exhibited highest inhibition rate (99%) at a concentration of 25 mg L-1 after 96 hours, with lowest inhibition rate (46%) obtained at a concentration of 5mg/L after 24 hours (Fig.1A). In comparison, Co-doped CuO NPs showed stronger growth inhibition against M. aeruginosa (Fig. 1B). The two highest concentrations (20 and 25 mg L-1) of Co-doped CuO NPs caused complete growth inhibition (100%), while the lowest inhibition rate (51%) was recorded after 24 hours.

These results agree with those of previous studies demonstrating that nano-copper carbon composite and CuO NPs could have severe inhibitory effects against microalgae and cyanobacteria [13, 25- 26].

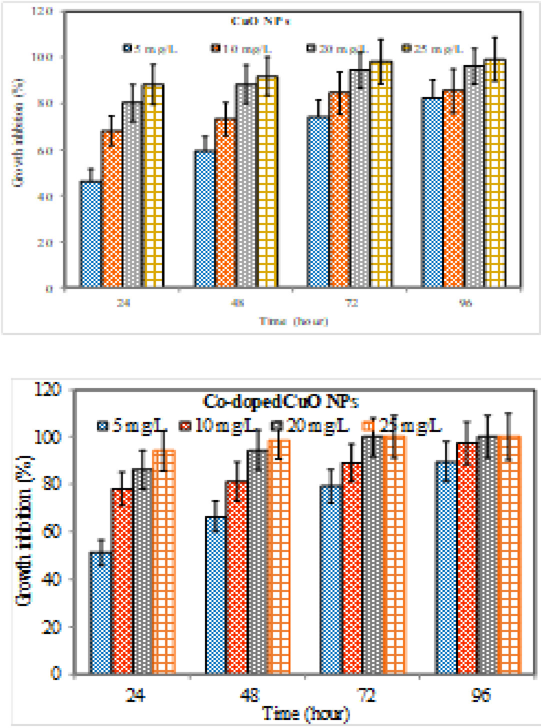

Fig. 1: Microcystis aeruginosa growth inhibition by CuO NPs (a) and Co-doped CuO NPs) at different concentrations for 96 hours.

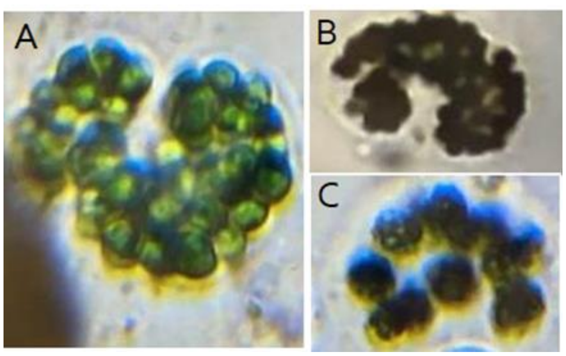

Fig. 2: Micrographs of M. aeruginosa cells in control cultures (A) and treated cultures with with 20 mg/L CuO NPs (B and C)

These studies attributed the inhibitory effect of these NPs to the mechanical action of CuO NPs, which aggregate on algal cell wall and damages cell membranes. This could be the inactivation mechanism of M. aeruginosa in our study, where NP aggregates were observed on the sheath and cells of this cyanobacterium (Fig. 2).

NPs adsorption is caused by electrostatic interaction between positively charged NPs and negatively charged surfaces of algal cells [27]. It is typical for M. aeruginosa [8,15, 28] and many other species of microalgae [29- 30] to exhibit this response to metallic nanoparticles.

Additionally, the linear regression of Probit analysis showed strong correlation between growth inhibition rate and the concentrations of either undoped or Co-doped CuO NPs ($R2= 0.956-1$). We also used the dose-response probit model to determine the median inhibitory concentration (IC50) for translating experimental findings into ecological context [31]. Based on the linear regression of Probit analysis. The results indicated that Co-doped CuO NPs exhibited higher efficiency on cyanobacterial growth inhibition with low IC50 values (0.3-4.6 mg/L) compared to undoped CuO NPs that showed higher IC50 values (0.8-5.6 mg/L). Also, the results revealed that IC50 values varied significantly ($P<0.05$) with the exposure time of M. aeruginoa to NPs. The highest the exposure time the lowest the IC50 (Table 1).

Table1: EC50 values estimated by Probit analysis for CuO Nps and Co-doped CuO NPs against Microcystis aeruginosa growth

Exposure time (hour)	IC_{50} (mg/L)	Regression Equation	R^2
CuO NPs			
24	5.63±1.1	y = 1.719x + 3.7106	0.9812
48	4.5±0.7	y = 1.7526x + 3.8574	0.8962
72	2.3±0.4	y = 1.7198x + 4.3968	0.9721
96	0.8±0.2	y = 1.0697x + 5.1075	0.8942
Co-doped CuO NPs			
24	4.6±1.2	y = 1.9882x + 3.6812	0.9562
48	2.8±0.5	y = 1.6528x + 4.2549	0.9953
72	1.3±0.3	y = 1.3786x + 4.8533	1
96	0.3±0.1	y = 1.0492x + 5.5313	1

The higher anti-cyanobacterial efficiency of Co-doped CuO NPs than undoped ones agree with the findings of earlier studies, is consistent with previous studies showing that co-doped CuO NPs exhibited better antibacterial activity than undoped ones [32- 33]. Those authors explained this by the fact that cobalt doping regulates the bandgap of CuO nanoparticles, increases surface area, reduces agglomeration, increases magnetism and enhances catalytic activity.

In addition to inactivation of cyanobacterial growth, both undoped and Co-doped CuO NPs showed a decrease in microcystin concentrations released into the culture medium upon cell lysis caused by these nanoparticles. As shown in Fig.3A, during the first 24 hours of the experiment, MC concentrations in the medium of CuO NP-treated cultures rose above those released in control cultures. Thereafter, they began to progressively decline over the course of the remaining experiment until they reached undatable levels for the highest two NP concentrations within 72 hours. Similarly, in M. aeruginosa cultures treated with Co-doped CuO NPs, MC concentrations increased throughout the first 24 hours and then gradually decreased. However, Co-doped CuO NPs showed a greater reduction in extracellular MCs than undoped ones, at 72 hours, MCs vanished entirely for all NP concentrations (Fig. 3B). These results indicate that undoped and Co-doped CuO NPs not only inactivated the cyanobacterial growth and caused cell lysis of M. aeruginosa, but also may be able to degrade or adsorb MC toxins released into the medium upon cell rupture. These findings corroborate those of earlier studies, demonstraing that CuO NPs and other nano-compoistes act as excellent photocatalytic and adsorption materials for the effective removal of cyanobacterial cells and MC toxins in practical applications [8, 15]. However, further in situ studies are needed to employ photocatalysis by undoped and doped CuO NPs to enhance the removal of algae in the coagulation phase in drinking water treatment plants.

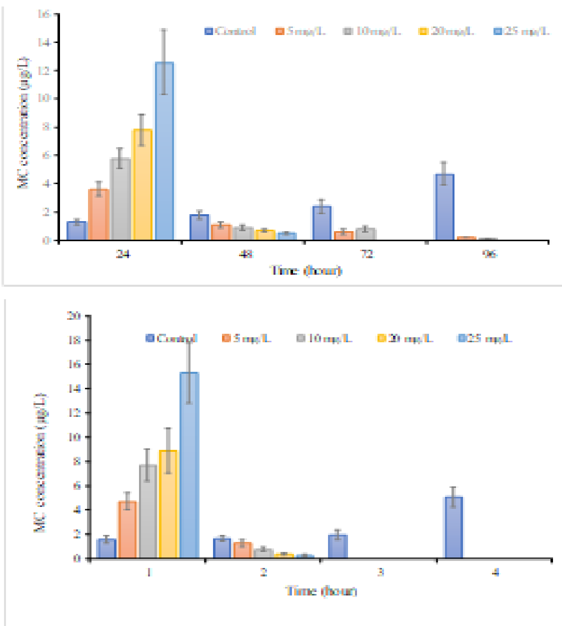

Fig. 3.: Effect of CuO NPs (a) and Co-doped CuO NPs (b) on microcystin concentrations released into the medium of Microcystis aeruginosa cultures for 96 hours.

4. Conclusion

In conclusion, our study clearly demonstrated a significant inhibitory effect of undoped and Co-doped CuO biosynthesized nanoparticles on the growth of Microcystis aeruginosa, with removal efficiency of 99-100% at a dose of 25 mg/L, respectively. This indicates that undoped CuO NPs are more effective for inactivation of cyanobacterial cells than Co-doped CuO NPs. Meanwhile, both undoped and doped NPs were also able to adsorb and remove MC toxins released upon cell lysis into medium. Because of their strong electrostatic attraction to the surfaces of cyanobacterial cells, these NPs will form nanoparticles-cyanobacteria -flocs, which settle in the sedimentation tank and are then easily removed with the sludge. Therefore, the study suggests using undoped and Co-doped CuO NPs as coagulants for simultaneous removal of cyanobacterial cells and microcystin toxins in drinking water treatment plants.

5. References

[1] C.S. Gil and S.H. Eom,” Two different anti-algal control mechanisms in Microcystis aeruginosa induced by robinin or tannin rich plants”, Chemosphere, vol. 323, pp. 138202, 2023.

[2] S. Huo, Z. He, C. Ma, H. Zhang, B. Xi, J. Zhang, , X. Li, , F. Wu, , H. Liu, “Spatio-temporal impacts of meteorological and geographic factors on the availability of nitrogen and phosphorus to algae in Chinese lakes”, J. Hydrol, vol. 572, pp. 380–387, 2019.

[3] L. Tarafdar, M. Mohapatra, P.R. Muduli, A. Kumar, D. R. Mishra, G. Rastogi,” Co-occurrence patterns and environmental factors associated with rapid onset of Microcystis aeruginosa bloom in a tropical coastal lagoon. J. Environ. Manag. 325, 116580, 2023.

[4] Y. Kong, Y. Peng, Z. Zhang, M. Zhang, Y. Zhou and Z. Duan,” Removal of microcystis aeruginosa by ultrasound: Inactivation mechanism and release of algal organic matter”, Ultrason Sonochem, vol. 56, pp. 447–457, 2019.

[5] M. R. Kelly, V. W. Moriarty, H. R. Kolar, G. A. Auger, M. E. Henderson, C. D. Watson and K. C. Rose, “A sequence of weather-driven hydrodynamic events stimulates the formation of harmful algal blooms on an oligotrophic lake”, Limnology and Oceanography, vol. 69(8), pp. 1826-1844, 2024.

[6] X. He, P. Wu, S. Wang, A. Wang, C. Wang and P. Ding, “Inactivation of harmful algae using photocatalysts: Mechanisms and performance”, J. Clean. Prod., vol. 289, pp. 125755, 2021.

[7] X. Zhu, G. Dao, Y. Tao, X. Zhan, H. Hu,” A Rev. Control Harmful Algal Blooms Plant-Deriv. Allelochem”, J. Hazard. Mater., vol. 401, pp. 123403, 2021.

[8] S. Lu, X. Li, B. Yu, J. Ding, Y. Zhong and H. Zhang, “Efficient Microcystis aeruginosa coagulation and removal by palladium clusters doped g-C3N4 with no light irradiation”, Ecotoxicology and Environmental Safety, vol.246, pp.114148, 2022.

[9] X. Xian, X. Li, C. Ye, K. Wan, M. Feng, C. Luo and X. Yu,” Higher sensitivity to Cu2+ exposure of Microcystis aeruginosa in late lag phase is beneficial to its control”, Water Research, vol. 214, pp. 118207, 2022.

[10] G. Nam, M.M. Mohamed, and J. Jung,” Novel treatment of Microcystis aeruginosa using chitosan-modified nanobubbles”, Environ. Pollut., vol. 292, pp. 118458, 2022.

[11] S. Zhou, Y. Yu, J. Sun, S. Zhu and J. Deng, “Oxidation of microcystin-LR by copper (II) coupled with ascorbic acid: kinetic modeling towards generation of H_2O_2”, Chem. Eng. J., vol. 333, pp. 443–450, 2018.

[12] F. Chen, Z. Xiao, L. Yue, J. Wang, Y. Feng, X. Zhu, Z.

Wang and B. Xing," Algae response to engineered nanoparticles: current understanding, mechanisms, and implications", Environ. Sci. Nano, vol. 6, pp.1026–1042, 2019.

[13] E. Solomonova, N. Shoman, A. Akimov and O. Rylkova, "Impact of copper oxide nanoparticles on the physiology of different microalgal species", Regional Studies in Marine Science, vol. 66, pp. 103128, 2023.

[14] P. Wang, L. Zhao, Y. Huang, W. Qian, X. Zhu, Z. Wang, Z. Cai," Combined toxicity of nano-TiO2 and Cd2+ to Scenedesmus obliquus: effects at different concentration ratios", J. Hazard Mater. 418, 126354, 2021.

[15] X. Gao, W. Feng, J. Zhang, H. Zhang and S. Huo," Synthesis of Cu^{2+} doped biochar and its inactivation performance of Microcystis aeruginosa: Significance of synergetic effect", Environmental Pollution, 334, 122186, 2023.

[16] J. Qi, H. Lan, S. Miao, Q. Xu, R. Liu, H. Liu and J. Qu, "KMnO4-Fe (II) pretreatment to enhance Microcystis aeruginosa removal by aluminum coagulation: Does it work after long distance transportation?", Water Res., vol. 88, pp. 127–134, 2016.

[17] S. A. Khan, S. Shahid, M. R. Sajid, F. Noreen and S. Kanwal," Biogenic synthesis of CuO nanoparticles and their biomedical applications: a current review", Int J Adv Res, vol. 5(6), pp. 925-946, 2017.

[18] A. Matei, G. Craciun, C. Romanitan, C. Pachiu and V. Tucureanu," Biosynthesis and Characterization of Copper Oxide Nanoparticles", Engineering Proceedings, vol. 37(1), pp. 54, 2023.

[19] S. Andra, S. K. Balu, J. Jeevanandham, M. Muthalagu, M. Vidyavathy, Y. S. Chan and M. K. Danquah, "Phytosynthesized metal oxide nanoparticles for pharmaceutical applications", Naunyn-Schmiedeberg's archives of pharmacology, 392, 755-771, 2019.

[20] F. Erci, R. Cakir-Koc, M. Yontem and E. Torlak, "Synthesis of biologically active copper oxide nanoparticles as promising novel antibacterial-antibiofilm agents" Preparative Biochemistry & Biotechnology, vol. 50(6), pp. 538-548, 2020.

[21] K. S. Siddiqi and A. Husen, "Current status of plant metabolite-based fabrication of copper/copper oxide nanoparticles and their applications: a review", Biomaterials Research, 24(1), 11, 2020.

[22] Bakr, A.," Algal flora, cyanotoxins and potential health hazards in fish farms in Sohag province", PhD thesis, Sohag University, Egypt, 2016.

[23] A. A. Hosny, B. El-Deeb, Z.A. Mohamed and E.M.M. Ibrahim," Biosynthesis of Fe_2O_3 and CuO Nanoparticles and Comparative Study for Dielectric Properties", Sohag J.Sci., vol. 9, pp. 206-210(2024). https://doi.org/10.21608/sjsci.2024.246871.1143

[24] W. W. Carmichael and J. An, "Using an enzyme linked immunosorbent assay (ELISA) and a protein phosphatase inhibition assay (PPIA) for the detection of microcystins and nodularins", Natural Toxins, vol. 7(6), pp. 377-385, 1999.

[25] I. Angela, K. Imbi, K. Kaja, B. Irina, A. Villem, S. Sandra, V. Heiki, K. Aleksandr, T. Tiina and H. Margit, "Size-dependent toxicity of silver nanoparticles to bacteria, yeast, algae, rrustaceans and mammalian cells in vitro", PLoS One, vol. 9(7), pp.102108, 2014.

[26] P. Zong, Y. Liu, H. Chen, S. Miao, K. Lian, C. Li and M. Zhang, "Inhibitory mechanism of nano-copper carbon composite on Microcystis aeruginosa", Algal Research, vol. 68, pp. 102877, 2022.

[27] A. S. Adeleye and A. A. Keller, "Interactions between algal extracellular polymeric substances and commercial TiO2 nanoparticles in aqueous media", Environmental science & technology, vol. 50(22), pp. 12258-12265, 2016.

[28] X. Wang, X. Wang, Z. Wei and S. Zhang," Potent removal of cyanobacteria with controlled release of toxic secondary metabolites by a titanium xerogel coagulant", Water Research, vol. 128, pp. 341-349, 2018.

[29] M. Sendra, I. Moreno-Garrido, J. Blasco and C. V. Araújo, "Effect of erythromycin and modulating effect of CeO2 NPs on the toxicity exerted by the antibiotic on the microalgae Chlamydomonas reinhardtii and Phaeodactylum tricornutum", Environmental pollution, vol. 242, pp. 357-366, 2018.

[30] C. Zhang, X. Chen, L. Tan and J. Wang, "Combined toxicities of copper nanoparticles with carbon nanotubes on marine microalgae Skeletonema costatum", Environmental Science and Pollution Research, vol. 25, pp. 13127-13133, 2018.

[31] L. H. Sylvers and C. J. Gobler, "Mitigation of harmful algal blooms caused by Alexandrium catenella and reduction in saxitoxin accumulation in bivalves using cultivable seaweeds", Harmful Algae, vol. 105, pp.102056, 2021.

[32] N. Thakur, K. Kumar, V. K. Thakur, S. Soni, A. Kumar and S. S. Samant, "Antibacterial and photocatalytic activity of undoped and (Ag, Fe) co-doped CuO nanoparticles via microwave-assisted method", Nanofabrication, vol. 7, pp. 62-88, 2022.

[33] P. S. Vindhya and V. T. Kavitha, "Effect of cobalt doping on antimicrobial, antioxidant and photocatalytic activities of CuO nanoparticles", Materials Science and Engineering, vol. 289, pp. 116258, 2023.

Journal of sustainable food, water, energy and environment

A comparison between the effect of zinc oxide and zinc oxide nannoparticles on the growth and some metabolic processes of *Cosmarium sp.*

***Asmaa Bakr*[1], *M.A. Awad* [2]**

[1]Botany and Microbiology Department, Faculty of Science, Sohag university, 82524, Egypt.
[2]Physics Department, Faculty of Science, Sohag university, 82524, Egypt.

Received: 15 Jan. 2025, Revised: 29 Jan. 2025, Accepted: 15 Feb. 2025 Published online: 1 Apr. 2025

Abstract: Bold Basal Media was used to culture the unicellular microalga *Cosmarium sp.* under carefully monitored conditions. In order to aid in microalga culture and extract useful compounds, we looked into biochemical characterizations applying nonmetals. Although the vast majority is cognizant of how harmful metal nanoparticles may be for microalgae, nanotechnology has a significant effect on a lot of other living organisms. The aim of this research is to evaluate the effects of zinc oxides and zinc oxide nannoparticles on *Cosmarium sp.* growth and induce resistance in order to improve the manufacture of high-value microalgae products. Zinc oxides and zinc oxide nannoparticles were added during its growth, with concentrations ranging from 0 to 300 mg/l. Studies comparing the effects of zinc oxide nanoparticles have shown that the treated cells accumulated more lipids and biomass than the non-exposed cells. The polymer's chloroform extract for *Cosmarium sp.* exposed to nannoparticles yielded eighteen distinct biodegradable chemicals, according to the results of GC/ MS analysis. Acetic acid, 2-methylpropyl ester (isobutyl acetate), Heptanol acid, nonanoic acid, and Heptanol acid were the main compounds found. Isobutyl acetyl citrate had the highest molecular weight of 402 and was the most prevalent compound with a total percentage of 29 and molecular weight of 116.08. *Cosmarium sp.* is capable of producing polyhydroxyalkanoate, which is about to be used extensively as a bioplastic, at different levels from zinc oxide nanoparticles.

Keywords: *Cosmarium sp* growth; Zinc oxides nanoparticles; Lipid content; growth rate; Poly hydroxyalkanoate

1. Introduction

In response to environmental stress, microalgae developed a variety of active compounds that they were biochemically and physiologically separated [1]. *Cosmarium sp.* is a freshwater alga that belong to the division of Chlorophyta [2]. An alga is a third-generation biofuel feedstock that is playing an increasingly major part in the global marketplace for renewable energy [3]. Because of its rapidly growing, high linear accumulation, and potential to engage in action to promote carbon neutralizing and microalgae production to reduce greenhouse gas emissions and air pollutants, the creation of biodiesel from plankton has been successful. Due to their capacity to convert nearly all food stock into biomass, microalgae can be thought of as the primary feedstock for the manufacture of biodiesel. Instead of utilizing energy for growth and development, their bodies have the ability to convert and store it so Microalga can be viewed as the main feedstock for biodiesel production [4-5]. Algae have 200 times more biomass per hectare than land-based crops [6]. A significant food source strong in vitamins, minerals, and proteins are microalgae, which in some areas have concentrations higher than those of conventional vegetable and animal protein sources. Metal and metal oxide nanoparticles are greater to their original state when it comes to enhancing the biological function of diverse species [7]. Reactive oxygen species (ROS) have been linked to nanoparticle toxicity to microalgae [8]. Oxidative stress-causing nanoparticles may encourage the growth of algae and the buildup of secondary metabolites [9]. The use of zinc oxide nanoparticles in this work to enhance *Cosmarium sp.* growth at various zinc oxide nanoparticle concentrations was an attractive approach. Protein, carbohydrate, and lipid contents, growth rate, biomass concentration, pigment concentration, and other factors were evaluated in order to assess how well metal nanoparticles worked in the process of producing high-value goods like polyhydroxyalkanoate from *Cosmarium sp.*

2. Material and Methods

2.1 Purification and Growth of *Cosmarium*

Cosmarium sp. was isolated by a streak-plate method from the waste water plant in Sohag, Egypt. Solid and liquid Bold Basel Medium are used to grow the culture, and a light/dark (length of 20ºC a12:12 h, with a cool white fluorescent illumination of Philips TL 40W and 140 μmol photons/m^2/s for about 15 days) incubator is used. Until Chlorophyta isolated single species, each species was grown in the same previous condition [10]. *Cosmarium sp.* was

* Corresponding author E-mail: Asmaabakr2011@yahoo.com Print ISSN 3062-5513 Online ISSN 3062-5521

grown in a medium containing metal oxide and metal oxide nannoparticles. The effect of zinc oxide and zinc oxide nannoparticles was evaluated by measuring the growth of the microorganism in each media using a different concentration range of 0-300 mg/l.

2.2 Metal Nanoparticle Synthesis and Characterization of Metal Nano Particles

The nanostructures of ZnO are synthesized using chemical vapor deposition (CVD) system, where Zn granules are placed in alumina boat in the center of the tubular furnace at temperature of 900^{o}C for 40 minutes. prior to the experiment an evacuation is carried out for the purpose of reducing the unwanted gas-phase reactions and improving the nanostructure uniformity. Argon and oxygen gases are allowed to flow with rates of 200 sccm and 20 sccm for the purpose of furnace purification and nanostructure growth. At the end of the experiment, the tubular furnace is cooled down to room temperature. The nanostructures' crystallographic structure was analyzed using X-ray diffractometry (Bruker D8 ADVANCE diffractometer) using Cu-Kα radiation (λ = 1.54056 Å). The size of the crystallite was determined using Debye-Scherrer's formula.

2.3 Determination of Specific Growth Rate

The *Cosmarium sp.* (μ) specific growth rate has been determined using the following formula.

$$\mu = \mathrm{Ln}\,(N_t / N_0)/T_t - T_0$$

where Nt and N0 represent the concentration of dry cell weight (g L^{-1}) at the beginning (T_0) and end (T_t) of the log phase, respectively.[11].

2.4 Determination of Biomass Concentration

The following formula was used to determine the biomass (g L^{-1}) of *Cosmarium sp.* cultivated in the presence of metal nanoparticles by measuring the optical density of samples at 600 nm (OD600) using UV-Vis spectrophotometers.

2.5 Chlorophyll-a Estimation

Centrifuged algae cells isolated overnight with 80% acetone were used to assess the chlorophyll concentration [12]. The extract was centrifuged for five minutes at 3000 x g, and a spectrophotometer was used to measure the amount of chlorophyll in the supernatant using the following equation.

$$\mathrm{Chl\ (mg/L)} = 8.02 \times \mathrm{OD663} + 20.21 \times \mathrm{OD645}$$

2.6 Carotenoids Estimation

After centrifuging, algae cells were treated with 60% w/w KOH. Ethyl ether was used to extract the mixture after it had been homogenized and heated to 40°C for 40 minutes [13]. The optical density was measured at 444 nm after the solvent was evaporated and then resuspended in acetone. The following formula was used to compute total carotenoids. Total carotenoids were calculated using the below equation.

$$\mathrm{Ct\ (mg/L)} = 4.32 \times \mathrm{OD444} - 0.0439$$

2.7 Determination of Total Lipids

Algal cells were collected by centrifugation, and they were then dried for lipid content analysis. A one-step extraction process had been used to remove the lipids [14]. Dried algal cells that were ultrasonic and chloroform were mixed with distilled water and methanol (2:1). After 30 minutes at 30°C in a water bath, the mixture was filtered through Whatman No. 1 filter paper. The layer of chloro-purified chloroform was transferred to a different tube holding the NaCl solution after being continuously evaporated to weight in a smoking cap at 60°C. The following formula was used to get the total dry weight lipid content.

Content of lipids (%) = $(m_2 - m_0)/m_1 \times 100$ where m0 represents the weight of the new screw cap tube when it is empty, m1 represents the weight of the dried algal cells, and m2 represents the weight of the new screw cap tube containing the dried lipids. Equation (g L^{-1} d^{-1}) was used to calculate lipid productivity.

Biomass productivity × Lipid content equals lipid productivity.

2.8 Gas Chromatography Mass Spectroscopy (GCMS)

Using an Agilent 5975 GC/MSD system, a gas chromatograph mass spectroscopy equipment was used to analyze the polyhydroxyalkanoate that was isolated from *Cosmorium sp.* column temperature was first maintained at 35 for 1.0 minute, then programmed to 20 at a rate of 25 / minute with holding time 1.0 minute, and finally at a rate of 10 / minute with holding time 2.0 minute. The column oven temperature was set to 60°C. The capillary column measured 30 m _ 0.25 mm (1.0μm film thickness).

2.9 Statistical Analysis

Using SPSS Statistics 21, mean and deviation from the mean data have been calculated for experiments conducted in triplicate. Three replicates (n = 3) of the data were analyzed using a single-way ANOVA, with $p < 0.05$ being considered statistically significant.

3. Results

The corresponding figure (Fig.1) shows results of XRD of the thin films deposited by CVD technique. Clearly, the nucleated species produced polycrystalline phases of Zn and ZnO (JCPDS files card no. 9008522 for Zn and 2107059 for ZnO). The relative peak integrated Intensity (RPII) of the mixed phases are calculated using equations:

$$RPII_{Zn} = \frac{I_{Zn}}{I_{Zn} + I_{ZnO}}$$

$$RPII_{ZnO} = \frac{I_{ZnO}}{I_{ZnO} + I_{Zn}}$$

That are resulted 69% for Zn and 31% for ZnO, confirming the main prominent of Zn phase. In this work the bi-structure of Zn/ZnO are intentionally synthesized by using short deposition time that are beneficial for water disinfection compared with the single phase of ZnO. Previously, it was reported that the existence of different phases in the structure prevent the electron-hole pair recombination hence enhancing the catalytic performance. Crystallite size (D) is calculated using Debye–Scherer formula:

$$D = \frac{0.9\,\lambda}{\beta\ Cos\theta_c}$$

where β is FWHM and λ is the wavelength of X-ray. The calculated crystallite size was 38.6 nm that confirms the granules size within the limits of nanometer. To inquire into how zinc oxide and zinc oxide nanoparticles behave differently into growth of *Cosmarium sp.* For seven days, *Cosmarium sp.* was grown in the presence of zinc oxide and zinc oxide nanoparticles. The growth rate of *Cosmarium sp.* that were tested and cultured in a solution of of zinc oxide and zinc oxide nanoparticles was determined and shown at figure2,3. The metal oxide and metal oxide nanoparticle concentrations that have been used were 0.0, 50, 100, 150, 200, 250, and 300 mg/L. The test organism was grown in the various concentrations for seven days. The results showed that, although the average rate of growth increased with increasing zinc oxide concentrations (p=0.05), it declined significantly with arising zinc oxide nanoparticle concentrations up to 300 mg/l (Figure 3). Biomass and chlorophyll-a content was assessed when they were cultivated with zinc oxide nanoparticles (fig. 4-7). Zinc oxides' has an inhibitory effects whereas zinc oxide nanoparticles' has an enhancing effects on microalgae. The values of biomass concentration also increased highly significantly up to the level of 250 mgl from metal oxides nanoparticles then they gradually up to the level of 300 mg/l ZnO nannoparticles, (p=0.05), above which a marked reduction in the values of biomass and chlorophyll-a content yield was reached. Biomass concentration had positive correlations with Specific growth rate of *cosmarium sp.* exposed to ZnO nannoparticles (r=0.681-0.989, p= 0.002-0.05), and Chl-a concentrations (r=0.603-0.777, p=0.038-0.045). Fig. 8,9. showed that once metal oxide nanoparticles were found, the lipid content in *Cosmarium sp.* increased. The chloroform extract of the polymer yielded eighteen distinct biodegradable chemicals, as indicated by the GCMS results of analysis. The most common compounds found were acetic acid, 2-methylpropyl ester (isobutyl acetate), which had a total percentage of 29 and a molecular weight of 116.08; other compounds included heptanoic acid, which had a percentage of 15, and nonanoic acid, which had a percentage of 11. The compound tributyl acetyl citrate had the highest molecular weight, which was recorded at 402. According to this research, *Cosmarium sp.* was able to synthesize PHAs, or polyhydroxyalkanoate. PHAs were first widely used in medicine in the 1970s. Thus, in 1974, the first biodegradable Vicryl surgical suture material made of chemically manufactured polymers was introduced to the pharmaceutical industry. A wide range of products (such as biodegradable surgical staples, screws, plates, pins, and cords; bioresorbable suture material and skin staples; wound and burn dressings; membranes for periodontal guided regeneration; surgical mesh endoprostheses; patches for surgical repair of intestinal and pericardial defects; mesh plugs for coloproctological applications and hernioplasty; vascular prosthetic implants; coronary stents; mesh tubes for nerve regeneration; artificial heart valves, and other medical devices) are either in use or in the process of being developed.

PHAs also bring characteristics as directed distribution, farther activity, less toxicity, and enhanced stability to new dosage forms utilized in pharmaceutics.

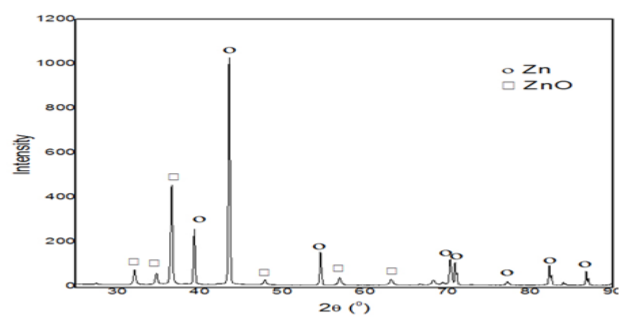

Fig. 1: XRD of Zno thin films.

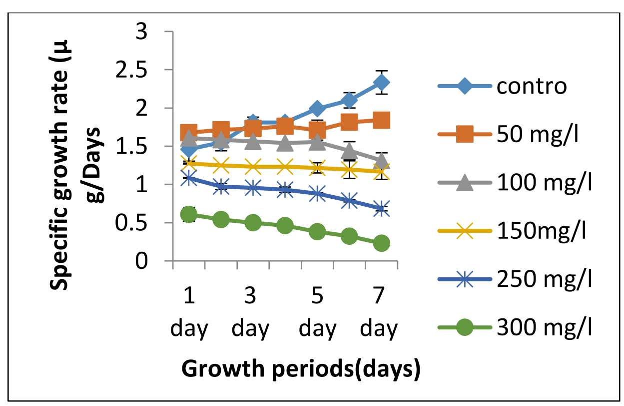

Fig. 2: The average rate of growth of *Cosmarium sp.* in the presence of zinc oxide.

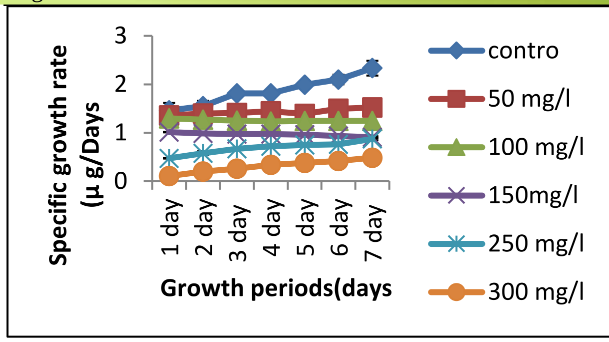

Fig. 3: The average rate of growth of *Cosmarium sp.* in the presence of zinc oxide nanoparticles.

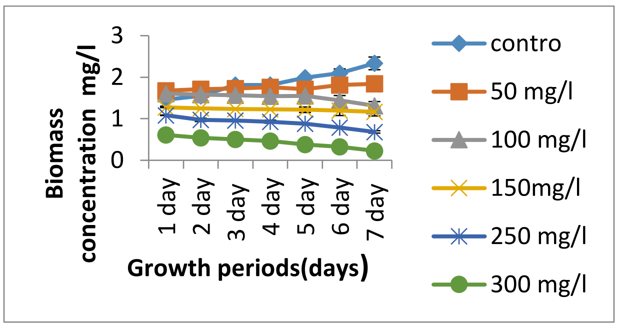

Fig. 4: Biomass concentration of *Cosmarium sp.* in the presence of zinc oxide.

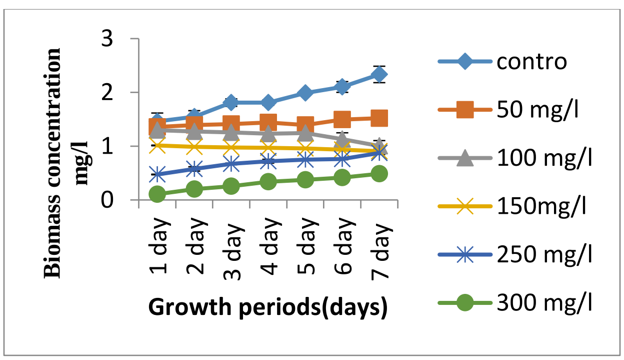

Fig. 5: Biomass concentration of *Cosmarium sp.* in the presence of zinc oxide nanoparticles.

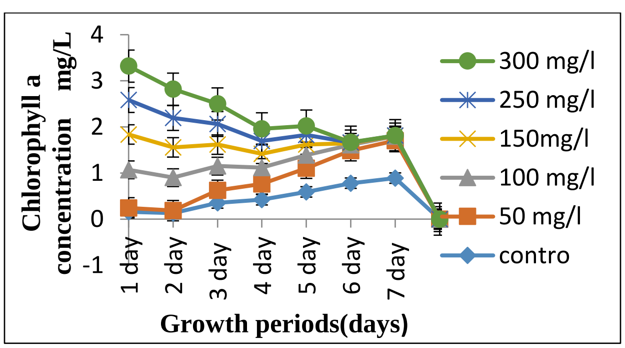

Fig. 6: Chlorophyll a concentration of *Cosmarium sp.* in the presence of zinc oxide.

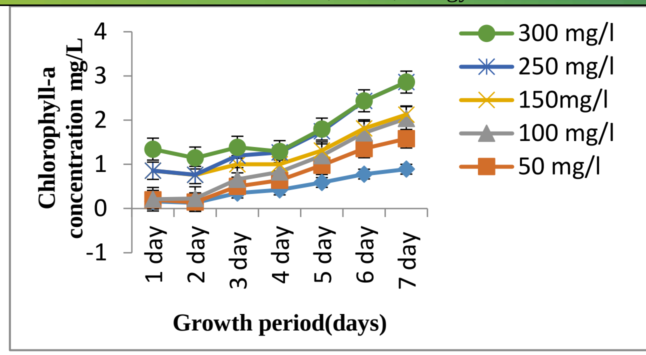

Fig. 7: Chlorophyll a concentration of *Cosmarium sp.* in the presence of zinc oxide nanoparticles.

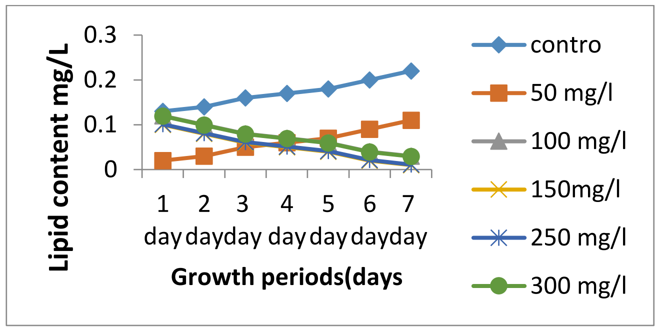

Fig. 8: Lipids content of *Cosmarium sp.* in the presence of zinc oxide.

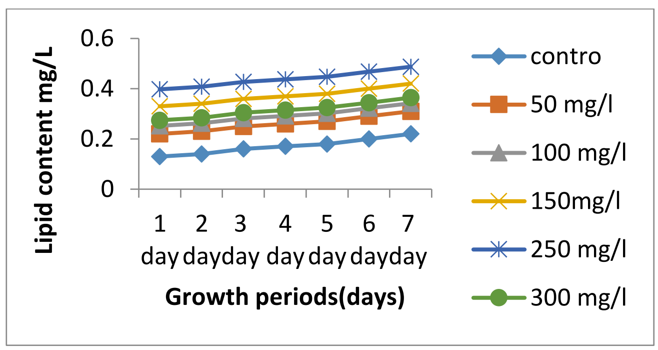

Fig. 9: lipids content of *Cosmarium sp.* in the presence of zinc oxide nannoparticles.

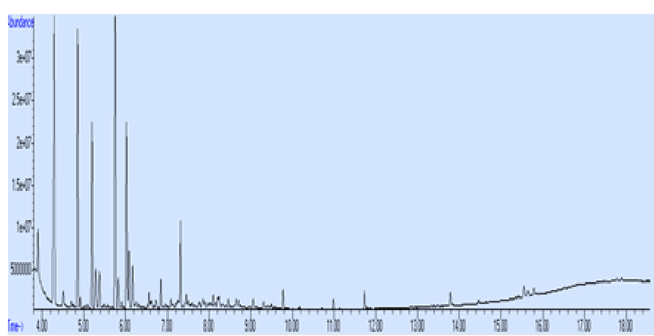

Fig. 10: Chromatogramme of MS peaks and linear retention indices were compared with the published data [15].

4. Discussion

The growth rate and biomass content of *Cosmarium sp.* were affected by concentrations of zinc metal oxides and metal oxide nannoparticles. The study revealed that zinc oxide nanoparticles on microalga had an expanding effect and that rate of growth, biomass, and biochemical characteristics of tested alga produced in the presence of metal oxide had inhibitory effects. The values of biomass concentration increased greatly up to 250 mg/l from metal oxide nanoparticles, then slightly dropped up to 300 mg/l ZnO nanoparticles, (p=0.05), after which a considerable decline in biomass production was observed. These results are in agreement with investigations[16], the microalgal cells were subjected to several concentrations of aqueous solutions containing zinc metal for a period of 15 days in order to assess growth inhibition [17].These concentrations of chlorophyll an also increased significantly up to the level of 250 mg/l from metal oxide nannoparticles, then reduced marginally up to the level of 300 mg/l ZnO nannoparticles, (p=0.05), above which a significant reduction in biomass yield values was seen. This is also strongly connected with *Cosmarium* growth rate (r=0.9), the degree in the reduction of growth and photosynthesis was much more pronounced than in metabolic rate (carbohydrate and protein metabolism) in most cases of *Cosmarium* that were treated with zinc oxides and zinc oxides nannaparticles. There were significant variations in concentration of chlorophyll under the effect of zinc oxides nannoparticles. (p<0.05). This is compatible with Navarro, E.; et al.2008 that showed the adsorption of NPs on the surface of algal cells results in a shading effect that affects algal photosynthesis. The shading effect caused by NPs affects the light, pigment and other conditions necessary for photosynthesis, weakening the algae absorption of light and thereby inhibiting the photosynthesis process [18-20].Reduced amounts of copper nanocarboxylates (20 to 40 mg L^{-1}) and selenium nanocarboxylates (0.07 to 0.2 mg L^{-1}) were added, and this promoted the growth of Chlorella and an increase in biomass in addition to the microalgae's chlorophyll content..The lipid content of algal biomass is presented in Figure 5. lipid content was observed increased on the 13th day ZnO nannoparticles exposed and control cultures, respectively It was interesting to note that the total lipid content in MNPS was 0.74 mg L^{-1} while it was just 0.15 mg L^{-1} in the control group. Another remarkable finding is an increase in microalgae lipid content, which has had a beneficial effect on *Cosmarium sp.* biomass and lipid content of 0.76 mg L^{-1}. High lipid yield and biomass productivity are critical for the viability of mass-culturing microalgae for the manufacture of biodiesel [21]. When carbon nanotubes, Fe_2O_3 nanoparticles, and MgO nanoparticles were present in Scenedesmus obliquus, both the neutral and total lipid concentrations increased [22]. The chloroform extract of the polymer yielded eighteen distinct biodegradable chemicals, as indicated by the GCMS analytical findings for *Cosmarium sp.* (Table 1). The melting peak of PHA was found to be 335oC and the total weight loss within this temperature range was 95%. The crystallinity of the PHA had been determined for standard PHB in previous reported [23].

5. Conclusion

The applications of metal nanoparticles to increase *Cosmarium sp.* metal resistance and increase the production of high-value byproducts like biomass, cellular pigments, and lipid from microalgae was assessed in this work. The extracted polymer was identified as PHA by GCMS analysis. The isolated PHA's thermal and mechanical properties were identical to those of regular PHA. As PHA producers, *Cosmarium sp.* has the added advantage of recycling waste carbon dioxide, a greenhouse gas, into plastics that are safe for the environment by employing solar energy. As a result, it's fair to assert that *Cosmarium sp.* can be used to produce PHA on a wider scale.

6. References

[1] A. Flores-Moya, E. Costas, E. Bañares-España, García-Villada, L. M. Altamirano, and V. López-Rodas, “Adaptation of Spirogyra insignis (Chlorophyta) to an extreme natural environment (sulphureous waters) through preselective mutations”, New Phytologist, pp. 655-661, 2005.

[2] S. A. Felisberto and L. Rodrigues, “Periphytic desmids in Corumbá reservoir, Goiás, Brazil: genus *Cosmarium Corda*”, Brazilian Journal of Biology, vol. 64, pp. 141-150, 2004.

[3] V. Patil, K.Q. Tran, and H.R. Giselrød, “Towards sustainable production of biofuels from microalgae”, International journal of molecular sciences, vol. 9, pp. 1188-1195, 2008.

[4] P.R. Pandit, M.H. Fulekar, and M.S.L. Karuna, “Effect of salinity stress on growth, lipid productivity, fatty acid composition, and biodiesel properties in Acutodesmus obliquus and Chlorella vulgaris”, Environmental Science and Pollution Research, vol. 24, pp. 13437-13451, 2017.

[5] S.A. Scott M.P. Davey, J.S. Dennis, I. Horst, C.J. Howe, D.J. Lea-and A.G. Smith, “Biodiesel from algae: challenges and prospects”, Current opinion in biotechnology, vol. 21, pp. 277-286, 2010.

[6] M. El Shafey and M. Asmaa, “Green synthesis of metal and metal oxide nanoparticles from plant leaf extracts and their applications: A review”, Green Processing and Synthesis, vol. 9, pp.304-339, 2020.

[7] G. Shraddha, T. Harshal, B. Prashant, D. Ganesh, " Biofuels: Successive production of biodiesel and bioethanol feedstock from the *Cosmarium sp.*", Int. J. Chem. Stud., vol. 6, pp. 550-554, 2018.

[8] Z. Yu, Q. Li, J. Wang, Y. Yu, Y. Wang, Q. Zhou, and P. Li, “Reactive oxygen species-related nanoparticle toxicity in the biomedical field”, Nanoscale research letters, vol. 15, pp. 1-14, 2020.

[9] M. He, Y. Yan, F. Pei, M. Wu, T. Gebreluel, S. Zou, and C. Wang, “Improvement on lipid production by Scenedesmus obliquus triggered by low dose exposure to nanoparticles”, Scientific reports, vol.7, pp.1-12, 2017.

[10] R. Y. Stanier, R. Kunisawa, M. Mandel and G. Cohen-Bazire, “The purification and properties of unicellular blue-green algae (order Chroococcales)”, Bact. Rev., vol. 35, pp. 171–205, 1971.

[11] G.A.K.D. Sibi, D.A. Kumar, T. Gopal, K. Harinath, S. Banupriya, and S.J.I.J.S.R.E.S.T. Chaitra, “Metal nanoparticle triggered growth and lipid production in Chlorella vulgaris”, International Journal of Scientific Research in Environmental Science and Toxicology, vol. 2, pp.1-8, 2017.

[12] E.W. Becker, “Microalgae: biotechnology and microbiology”, Cambridge University Press, Vol. 10,1994 .

[13] J. N. C. Whyte, “Biochemical composition and energy content of six species of phytoplankton used in mariculture of bivalves”, Aquaculture., vol. 60, pp.231-241, 1987.

[14] J. Folch, M. Lees, G. H. S., “Stanley A simple method for the isolation and purification of total lipids from animal tissues”, J. Biol. Chem., vol. 226, pp. 497-509, 1956.

[15] M. L. Adams, M. Pan, and J. Pawliszyn, “Determination of fatty acids using solid phase microextraction”, Analytical Chemistry, vol. 67, pp.4396-4403,1995.

[16] A. R. Ribeiro, C. Olga Nunes, F. R. Manuel Pereira, and M. T. Silva. "An overview on the advanced oxidation processes applied for the treatment of water pollutants defined in the recently launched Directive 2013/39/EU", Environment international, vol. 75, pp. 33-51, 2015.

[17] D. Kumar, P. Santhanam, S. Ananth, A. S. Devi, R. Nandakumar, B. B. Prasath, and P. Ananthi,” Effect of different dosages of zinc on the growth and biomass in five marine microalgae”, International Journal of Fisheries and Aquaculture, vol. 6, pp. 1-8, 2014.

[18] F. Perreault, A. Oukarroum, S. P. Melegari, W. G. Matias and R. Popovic, “Polymer coating of copper oxide nanoparticles increases nanoparticles uptake and toxicity in the green alga Chlamydomonas reinhardtii”, Chemosphere, vol. 87, pp. 1388–1394, 2012.

[19] X. Li, K. Schirmer, L. Bernard, L. Sigg, S. Pillai and R. Behra,” Silver nanoparticle toxicity and association with the alga Euglena gracilis”, Environmental Science: Nano., vol. 2, pp. 594–602, 2015.

[20] X. Chen, C. Zhang, L. Tan, and J. Wang, “Toxicity of Co nanoparticles on three species of marine microalgae”, Environmental Pollution, vol. 236, pp. 454–461, 2018.

[21] J. Jena, N. Pradhan, V. Aishvarya, R. R. Nayak, B. P. Dash, L. B. Sukla, P. K. Panda and B.K. Mishra, “Biological sequestration and retention of cadmium as CdS nanoparticles by the microalga Scenedesmus-24”, Journal of Applied Phycology, vol. 27, pp. 2251–2260, 2015.

[22] P. Chen, B. A. Powell, M. Mortimer and P.C Ke, “Adaptive interactions between zinc oxide nanoparticles and Chlorella sp.”, environmental science and technology, vol. 46, pp. 12178–12185, 2012.

[23] S. Ansari and T. Fatma, “Cyanobacterial polyhydroxybutyrate (PHB), screening, optimization and characterization”, PLoS ONE., vol. 11, pp. 158–168, 2016.

Journal of sustainable food, water, energy and environment

Environmental Impact Assessment of the two-spotted spider mite , Tetranychus urticae Koch on Phaseolus vulgaris L plants as in Light of temperature Changes in Sohag Governorate

A. S. S. Desoky[1], M. W. A. Negm[2], Mai M. M. Saleh[1,3]

[1]Plant protection Department, Faculty of Agriculture, Sohag University, Egypt
[2]Plant Protection Department, Faculty of Agriculture, Assiut University, Egypt
[1,3]Faculty of Graduate Studies and Environmental Research, Sohag University, 82524 Sohag, Egypt

Received: 28 Jan. 2025, Revised: 15 Feb. 2025, Accepted: 1 Mar. 2025 Published online: 1 Apr. 2025

Abstract: Climate change and global warming are of great concern to agriculture worldwide and are among the most discussed issues in today's society. Climate parameters such as increased temperatures, rising atmospheric CO_2 levels, and changing precipitation patterns have significant impacts on agricultural production and on agricultural insect pests. Changes in climate can affect insect pests in several ways. As a result, there is a serious risk of crop economic losses, as well as a challenge to human food security. As a major driver of pest population dynamics, climate change will require adaptive management strategies to deal with the changing status of pests. Several priorities can be identified for future research on the effects of climatic changes on agricultural insect pests. The popoulation abundance of the two-spotted spider mite, Tetranychus urticae infesting Phaseolus vulgaris L plants in upper Egypt was studied during spring plantations of 2015 and 2016 season. The obtained results showed that, the spider mite population fluctuated in its density during the whole season of both studied years with a peak number occurrence the end of season (May 30), when plant age was 90 day-olds when temperature and relative humidity were in moderate levels. Also, the current study showed that, Phaseolus vulgaris L plants severely affected by the pest in addition to the few numbers of predators were observed during this season. The temperature and relative humidity, in addition to the plant age probably play an important role in the infestation other than the biotic factors (predators). Accordingly, further studies are required to set up and confirm the main factors affecting the population of this pest. This study is useful for determining the timing of the control program for the two-spotted spider mite, Tetranychus urticae infesting Phaseolus vulgaris L plants during spring plantations.
Keywords: Tetranychus urticae ;Phaseolus vulgaris L plants ;spring plantations; temperature; relative humidity

1. Introduction

Phaseolus vulgaris L. which commonly known in Egypt as Phasolia is a member of Fabaceae (Papilionaceae) family. It is known as Common, Snap, Kidney, French or Haricot beans [1-3] The Kidney beanis a tender annual, cultivated as a food crop in many parts of the world including the temperate, sub-tropical and tropical zones.

It plays an important role in human nutrition as a cheap source for protein, carbohydrates, vitamins and minerals and is considered one of the most important vegetable crops cultivated in Egypt for exportation and for local market as well.

The immature pods of these beans are also an important food source in many locations around the world, where they are known as green beans, snap beans, French beans or string beans. They are important foods in most tropical and subtropical countries of the world and they are second only to cereals as a food source for humans and animals [4].

One of the most important pests in commercial crops worldwide is the polyphagous, two-spotted spider mite, Tetranychus urticae Koch. This mite is able to alter the physiological processes of plants, reducing the area of photosynthetic activity and causing the abscission of leaves in severe infestations [5].

The cost of damages caused by this pest in crops such as beans, citrus, cotton, avocado, apples, pears, plums, and many other horticultural and ornamental crops are estimated at over USD$ 4500 per hectare. Such costs correspond to 30% of the total cost of pesticides in crops of ornamental flowers. This constitutes a spending of almost 62% of the global market value on T. urticae Koch control based on data of 2008 [6]. The main tools used to control this pest are chemically synthesized acaricides.

* Corresponding author E-mail: abdelalem2011@gmail.com Print ISSN 3062-5513 Online ISSN 3062-5521

Abou El-Saad [7] studied the numerical density of phytophagous mites (i. e. Tetranychus urticae Koch, (Acari: Tetranychidae) inhabiting common bean, Phaseolus vulgaris L. The data indicated that T. urticae Koch and T. cucurbitacearum (Sayed) infested Phaseolus vulgaris L Sarwar [8] studied the population density of the two-spotted spider mite, Tetranychus urticae Koch (Tetranychidae), on Phaseolus vulgaris L. which was the pest of agricultural crops that could potentially be controlled by the predatory mite.

Basha et al. [9] obtained the two- spotted spider mite, Tetranychus urticae Koch. (Tetranychidae) on common been Phaseolus vulgaris were conducted during 2016 and 2017 seasons at Kom-Hamada district, Beheira governorate, Egypt. The spider mite occurred in relatively few numbers of 1.60 & 0.84 individuals per leaf at the late February of both seasons, respectively and the populations increased and reached the highest density of 18.20 and 20.60 individuals per leaf. Basha et al. [9] found the initial incidence of the spider mite occurred in relatively few numbers of 1.60 & 0.84 individuals per leaf. Temperature appeared to be the most environmental factor affecting population build-up of this pest on the investigated crop at Kom-Hamada district, Beheira governorate, Egypt.

Allam [10] investigated three acaricides Indo 50% EC; Challenger 36% SC and Ortus 5% SC for controlling the phytophagous mites, Tetranychus urticae Koch at Gharbia Governorate on kidney bean plants. Ammar et al. [11] evaluated the efficiency of Abamectin against Tetranychus urticae (Koch) infesting green bean (Phaseolus vulgaris) on the autumn. Abou-Zaid et al. [12] studied that the bio pesticide Abamectin1.8 EC.+ mineral oil Cable against the eggs, immature and adults of Tetranychus urticae Koch (Acari: Tetranychidae) infesting two cultivars of both P. vulgaris (Hama and Bolista) under net house conditions at Beheira Governorate. Therefore, the current study was carried out to show the effect of weather factors, plant age and plant levels on the population density of the mite pest on cucumber plants during spring plantation.

2. Materials and Methods

The present study was conducted at the experimental farm of the Faculty of Agriculture (Al-Kawamil city), Sohag University during two successive spring seasons of 2015 and 2016. An area of about quarter feddan (1050 m²) was divided into 100 plots (each was 3×3.5m). The spring plantations were sown on March 1 of both years. Normal agricultural practices free from pesticides treatment were followed. Sampling started two weeks after planting data, and continued fortnightly until harvest. Nine cucumber leaves from five randomized chosen plots of different sides with three replicates at three plant levels (top, middle and bottom) were taken fortnightly leaves were put in tightly closed paper bags labeled with necessary informations, then translocated into the laboratory for examination by using stereoscopic binocular microscope of 40-100 times magnification force. The number of Tetranychus urticae motile stages were counted and recorded. Temperature (°C), (max. and min.) and relative humidity (%) max and min were obtained from the meteorological station of the experimental farm of the Faculty of Agriculture, Sohag University. Simple correlation co-efficient (r) was calculated in order to study the effect of weather factors, plant age and plant levels on the population density of the two-spotted spider mite, Tetranychus urticae motile stages on cucumber plants during the spring planations of both years (2015 and 2016).

3. Results and discussions

In general, the current study showed that the number of days from the date of cucumber planting to harvest took about 90 days in spring plantations during the two studied years (2015 and 2016) in Al-Kawamil city, Sohag Governorate. The population fluctuations of T. urticae motile stages are presented in Table (1). The first appearance of the mite was recorded on March 16th, when plant age was 16 day-olds. The mite density begins with relatively high abundance 28.26 individuals / 9 plant leaves (2015) and 32.4 individuals / 9 leaves (2016), then increased gradually by the end of (March 30) was recorded 32.7 individuals (2015) and 38.9 individuals (2016), when max. and min. of both temperature and relative humidity were 25, 14°C; 38, 22 %R.H. (2015) and 25, 11°C and 55,15 % R.H. (2016), respectively. Then, the population of the pest fluctuated in high density until the end of the season. (May 30) in both years, with an average number of 81.96 individuals / 9 plant leaves of max .and min. of both temperature and relative humidity were 32 and 19 °C; 36 and 15% R.H. (2015 season), respectively. In 2016 season, the number was 86.6 individuals / 9 plant leaves at 35 and 35 and 19 °C; 45 and 10 % R.H.

Data in Table (2) showed the correlations (r) between the pest population recovered from the three plant levels of P. vulgaris in spring plantations of 2015 and 2016 seasons with (max. and min.) temperature and relative humidity. Highly significant positive correlations were recorded between the pest population on the three plant levels (top , middle and bottom) and (max.and min) temperature, where r =0.956 , 0.959 ,0.957 ,0.969 ,0.972 ,0.970 during spring plantations of 2015 season , respectively .Whereas the relationship with R.H.% ,were highly significant negative with max. R.H. (r = -0.962,-0.959, 0.961) on the three plant levels, and negative significant ones with min. R.H.(r = -0.720, -0.727, -0.722) on the three plant levels of spring plantations of , 2016 season ,respectively. The same trend of results was also found with few differences in 2016 spring season.

Sampling date		Mean No. of mites /9leaves	Temp. (°C)		R.H. (%)	
			Max.	Min.	Max.	Min
2015	March 15	96.7	25	12	50	18
	March 30	123.9	25	14	38	22
	April 15	150.65	24	11	45	13
	April 30	171.4	36	21	42	8
	May 15	201.7	35	18	34	7
	May30	280.9	32	19	36	15
2016	March 15	120.96	23	11	48	19
	March 30	132.9	25	11	55	15
	April 15	149.1	32	16	35	11
	April 30	174.5	35	17	24	6
	May 15	211.2	43	26	12	4
	May30	286.8	35	19	45	10

Table 1: Population fluctuations of T. urticae motile stages on P. vulgaris plant in spring plantations of 2015 and 2016 seasons:

- Temp. Max. = Temperature Maximum and Temp. Min. = Temperature Minimum
- R.H. Max. = Relative humidity Maximum and R.H. Min. = Relative humidity Minimum

Factors	No. of mite /9 leaves					
	2015			2016		
	Top leaves	Middle leaves	Bottom leaves	Top leaves	Middle leaves	Bottom leaves
Temp. Max.	0.956**	0.959**	0.957**	0.967**	0.940**	0.949**
Temp. Min.	0.969**	0.972**	0.970**	0.997**	0.986**	0.990**
R.H. Max.	-0.962**	-0.959**	-0.961**	-0.830**	-0.778*	-0.794**
R.H. Min.	-0.720*	-0.727*	-0.722*	-0.882**	-0.837**	-0.851**

Table 2: Simple correlations coefficient (r) between number of T. urticae (motile stages) on three P. vulgaris plant levels and the temperature, relative humidity during two growing spring seasons 2015 and 2016.

** Correlation is highly significant at the 0.05 level.
* Correlation is significant at the 0.01 level.

The spider mite T. urticae showed non-significant positive correlation with average temperature and a non-significant negative correlation with average relative humidity by Ammar and Abolmaaty [13] during two successive seasons on 2015 and 2016at cucumber crop. Our result was similar with Rinkikumari and Shukla [14] were reached to the spider mite showed non-significant negative correlation with average temperature and a non-significant positive correlation with average relative humidity. In poly house, throughout the crop season the distribution of T. urticae was higher on top strata followed by middle strata and bottom strata which studied the population dynamics of two spotted red spider mite, T. urticae.

From the study, it can be conculated that the two-spotted spider mite, T. urticae is a very crucial pest infesting P. vulgaris plants in Egypt. The present results showed that the pest started to infest early age plants (15 day-old). Temperature and relative humidity, as well as plant age, may play an important role in infection other than biotic factors (predators). Accordingly, further studies are required to prepare and confirm the main factors affecting the population of this pest. It is recommended to control weeds before planting both in and around the fields as they are the main source of infestation, and we can benefit from this study by determining the timing of the control program for the two-spotted spider mite infesting P. vulgaris plants during this period.

5. References

[1] S.P. Singh, "Common Bean: Improvement in the Twenty-First Century", Kluwer Academic Publishers, _@London, pp. 2-7, 1999.

[2] B.P. Pandey," Economic Botany. S. Chand and Company Ltd. Ram Nagar, 6th Ed., New Delhi, India, pp. 32, 2003.

[3] F.A. Bisby, Y.R. Roskov, T.M., D. Orrell, L.E. Nicolson, N. Paglinawan, P.M. Bailly, T. Kirk, G. Bourgoin, Baillargeon and D. Ouvrard, "Species 2000 and ITIS Catalogue of life", Species 2000: Reading, UK, 2011.

http: // www.catalogueoflif.org/col.

[4] P.H. Graham, and C.P. Vance, "Legumes: Importance and constraints to greater use", Plant Physiology, vol. 131(1), pp. 872–877, 2003.

[5] S. Kumari, U. Chauhan, A. Kumari, G. Nadda, "Comparative toxicities of novel and conventional acaricides against different stages of Tetranychus urticae Koch (Acarina: Tetranychidae)", J. Saudi Soc. Agric. Sci., vol 16, pp. 191–196, 2017.

[6] T. Van Leeuwen, L. Tirry, A. Yamamoto, R. Nauen and W. Dermauw," The economic importance of acaricides in the control of phytophagous mites and an update on recent acaricide mode of action research. Pestic. Biochem. Physiol. Vol. 121, pp. 12–21, 2015.

[7] A.K. Abou El-Saad, "Mites infesting three vegetable crops in Assiut governorate", J. Plant Prot. and Path., Mansoura Univ., vol. 6 (2), pp. 399 – 406, 2015.

[8] M. Sarwar, "Influence of host plant species on the development, fecundity and population density of pest Tetranychus urticae Koch (Acari: Tetranychidae) and predator Neoseiulus pseudolongispinosus (Xin, Liang and Ke) (Acari: Phytoseiidae)", New Zealand Journal of Crop and Horticultural Science, vol. 42 (1), pp.1020, 2014.

[9] M. A. Basha, E.M. Mostafa, M. Y. Hendawi, M. Eleawa, and A. A. Shalaby, "Seasonal abundance of the two- spotted spider mite Tertranychus urticae koch on common bean Phaseolus vulgaris L.", Life Science Journal., vol. 15 (9), pp. 42-48, 2018.

[10] S. A. Allam, "Evaluation of some acaricides against the two spotted spider mite, Tetranychus urticae koch and its predacous mites on kidney bean plants at el-Gharbia governorate", Egypt. J. Plant Prot. and Pathology, Mansoura Univ., vol. 2 (6), pp. 637 – 643, 2011.

[11] M.I. Ammar, S.M. Abozeid, and T.A. Abd Elrahman," Evaluation the Number, duration generation and efficiency of Abamectin against some pests infesting green bean (Phaseolus vulgaris L.) under field condition", Egypt. Acad. J. Biolog. Sci., vol. 10 (3), pp. 89–98, 2017.

[12] A.M.M. Abou-Zaid, S.A. Yassin, M.H. Mahgoub and M.S. Kamel, "Efficacy of predatory phytoseiid mites and biopesticides for controlling Tetranychus urticae (Acari: Tetranychidae) infesting Phaseolus vulgaris. Egypt", J. Plant Prot. Res. Inst., vol. 2 (2), pp.: 339 – 351, 2019.

[13] M.I. Ammar, and S.M. Abolmaaty," Effect of different colors Mulch on population density of pome pests infesting Cucumber plants and on Cucumber yield. Egypt. Acad. J. Biolog. Sci., vol. 9(4), pp. 153–162, 2016.

[14] C. Rinkikumari and A. Shukla, "Population dynamics of two spotted red spider mite, Tetranychus urticae koch on french bean under poly house condition", J. Exp. Zool. India., vol. 19(1), pp.1577-1579, 2016.

